AD-A130 041 MECHANISMS OF CORROSION FATIGUE IN HIGH STRENGTH I/M (INGOT METALLURGY) A..(U) LEHIGH UNIV BETHLEHEM PA INST OF FRACTURE AND SOLID MECHANICS.. R P WEI ET AL. 1/1

UNCLASSIFIED FEB 83 IFSM-83-114 AFOSR-TR-83-0560 F/G 11/6 NL

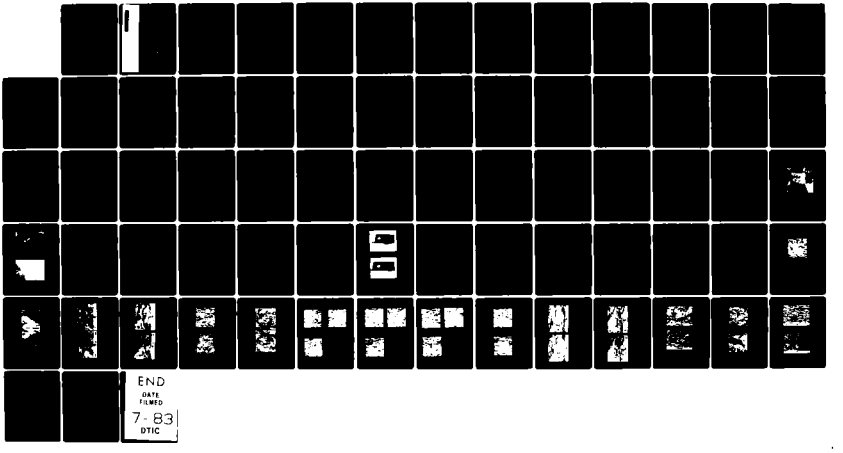

END

DATE FILMED

7-83

DTIC

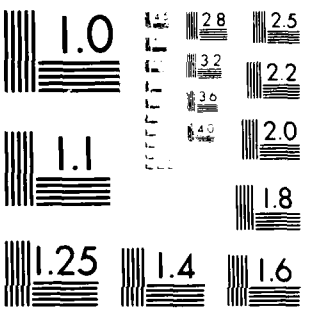

AFOSR-TR- 83-0560

IFSM-83-114

LEHIGH UNIVERSITY

INSTITUTE OF FRACTURE AND SOLID MECHANICS

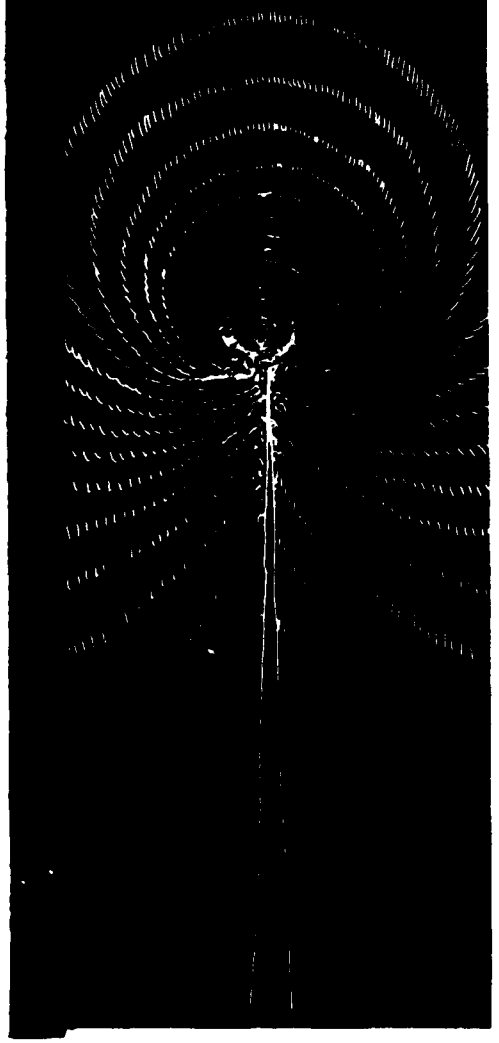

MECHANISMS OF CORROSION FATIGUE IN HIGH STRENGTH I/M AND P/M ALUMINUM ALLOYS

by

R. P. Wei
Lehigh University

and

P. S. Pao
McDonnell Douglas Research Laboratories

February, 1983

Technical Report No. 2

Air Force Office of Scientific Research

Contract No. F49620-81-K-0004

MECHANISMS OF CORROSION FATIGUE IN HIGH STRENGTH I/M AND P/M ALUMINUM ALLOYS

by

R. P. Wei
Lehigh University

and

P. S. Pao
McDonnell Douglas Research Laboratories

February, 1983

Technical Report No. 2

AIR FORCE OFFICE OF SCIENTIFIC RESEARCH

(Contract No. F49620-81-K-0004)

UNCLASSIFIED

SECURITY CLASSIFICATION OF THIS PAGE (When Data Entered)

REPORT DOCUMENTATION PAGE		READ INSTRUCTIONS BEFORE COMPLETING FORM
1. REPORT NUMBER AFOSR-TR- 83-0560	2. GOVT ACCESSION NO. AD-A130 041	3. RECIPIENT'S CATALOG NUMBER
4. TITLE (and Subtitle) MECHANISMS OF CORROSION FATIGUE IN HIGH STRENGTH I/M AND P/M ALUMINUM ALLOYS		5. TYPE OF REPORT & PERIOD COVERED Technical 6. PERFORMING ORG. REPORT NUMBER Technical Report No. 2
7. AUTHOR(s) R. P. Wei, Lehigh University P. S. Pao, McDonnell Douglas Research Laboratories		8. CONTRACT OR GRANT NUMBER(s) Contract No. F49620-81-K-0004
9. PERFORMING ORGANIZATION NAME AND ADDRESS Lehigh University Bethlehem, PA 18015		10. PROGRAM ELEMENT, PROJECT, TASK AREA & WORK UNIT NUMBERS 6 1102F 2306/H1
11. CONTROLLING OFFICE NAME AND ADDRESS Air Force Office of Scientific Research Bolling Air Force Base, DC 20332		12. REPORT DATE February, 1983 13. NUMBER OF PAGES 68
14. MONITORING AGENCY NAME & ADDRESS(if different from Controlling Office)		15. SECURITY CLASS. (of this report) Unclassified 15a. DECLASSIFICATION/DOWNGRADING SCHEDULE

16. DISTRIBUTION STATEMENT (of this Report)

This document has been approved for public release; its distribution is unlimited.

17. DISTRIBUTION STATEMENT (of the abstract entered in Block 20, if different from Report)

18. SUPPLEMENTARY NOTES

19. KEY WORDS (Continue on reverse side if necessary and identify by block number)

Aluminum alloy; corrosion fatigue; fracture mechanics; microstructure; environmental effects.

20. ABSTRACT (Continue on reverse side if necessary and identify by block number)

High strength aluminum alloys are employed extensively in the primary structure of current and projected Air Force and civilian aircraft. The service lives and reliability of these aircrafts depend to a great extent on the corrosion fatigue resistance of the structural alloys. Significant efforts are underway to develop powder metallurgy (P/M) alloys that would provide improved corrosion fatigue resistance along with improve-

DD FORM 1 JAN 73 1473 EDITION OF 1 NOV 65 IS OBSOLETE
S/N 0102-014-6601

UNCLASSIFIED

SECURITY CLASSIFICATION OF THIS PAGE (When Data Entered)

ments in other mechanical properties. The objective of this study is to understand the chemical and metallurgical aspects of environmentally assisted fatigue crack growth (or corrosion fatigue) that can serve (i) as a basis for guiding the development of new and improved alloys, and (ii) as a basis for developing rational design procedures for service life predictions. A coordinated fracture mechanics, surface chemistry and materials science approach is used. The research is being performed by Lehigh University with technical support by McDonnell Douglas Research Laboratories.

The second year effort was devoted to the study of 7075-T651 (I/M) alloy, and X7091-T7E69 and X7091-T7E70 (P/M) alloys. The kinetics of fatigue crack growth, as a function of water vapor pressure and for water vapor-oxygen mixtures, and the accompanying fractographic observations are described and discussed. Comparison between the I/M and P/M alloys are given. The implications of these results in terms of the current and proposed models for environmentally assisted fatigue crack growth are discussed. Plans for the third year of research are also described.

TABLE OF CONTENTS

SECOND ANNUAL TECHNICAL REPORT
(AFOSR Contract No. F49620-81-K-0004)

MECHANISMS OF CORROSION FATIGUE IN HIGH STRENGTH I/M AND P/M ALUMINUM ALLOYS

by

R. P. Wei
Lehigh University
and
P. S. Pao
McDonnell Douglas Research Laboratories

ABSTRACT

High strength aluminum alloys are employed extensively in the primary structure of current and projected Air Force and civilian aircraft. The service lives and reliability of these aircrafts depend to a great extent on the corrosion fatigue resistance of the structural alloys. Significant efforts are underway to develop powder metallurgy (P/M) alloys that would provide improved corrosion fatigue resistance along with improvements in other mechanical properties. The objective of this study is to understand the chemical and metallurgical aspects of environmentally assisted fatigue crack growth (or corrosion fatigue) that can serve (i) as a basis for guiding the development of new and improved alloys, and (ii) as a basis for developing rational design procedures for service life predictions. A coordinated fracture mechanics, surface chemistry and materials science approach is used. The research is being performed by Lehigh University with technical support by McDonnell Douglas Research Laboratories.

The second year effort was devoted to the study of 7075-T651 (I/M) alloy, and X7091-T7E69 and X7091-T7E70 (P/M) alloys. The kinetics of fatigue crack growth, as a function of water vapor pressure and for water vapor-oxygen mixtures, and the accompanying fractographic observations are described and discussed. Comparison between the I/M and P/M alloys are given. The implications of these results in terms of the current and proposed models for environmentally assisted fatigue crack growth are discussed. Plans for the third year of research are also described.

1.0 Introduction

This report describes work performed on "Mechanisms of Corrosion Fatigue in High Strength I/M and P/M Aluminum Alloys". High-strength aluminum alloys are used extensively in the primary structures of military and commerical aircraft. These alloys are based on either the Al-Cu system (2XXX series alloy) or the Al-Zn-Mg or Al-Zn-Mg-Cu systems (7XXX series alloys). Because these aircraft parts are exposed to chemically-active service environments, such as moisture and runway salt sprays, their useful lives and reliability depend on the corrosion fatigue resistance of the structural alloys. The need for improved performance, greater structural reliability, and longer service lives in advanced aircraft designs have called for new and improved alloys that combine high strength, good fracture toughness, and improved corrosion fatigue resistance. Significant improvements in these properties have been achieved on alloys produced by ingot metallurgy (I/M alloys) during the past decade through better ingot processing, improved compositions, and the use of thermo-mechanical treatments.

In recent years, powder metallurgy (P/M) or rapid solidification processing (RSP) have emerged as alternative routes for the optimization of aluminum alloy properties and for the development of new alloys. High solidification rates associated with the production of P/M alloys minimize segregation, reduce significantly the size and volume fraction of constituent particles, and refine and homogenize the microstructures. Rapid solidification processing also offers considerable freedom in alloying and thus permits the processing of new and novel compo-

sitions that cannot be handled readily by ingot (I/M) techniques. These alloys promise to provide high strength, along with good fracture, fatigue and stress corrosion cracking resistances, and are undergoing considerable development. The alloy development effort is expected to accelerate in the coming years.

The resistance of high-strength I/M and P/M aluminum alloys to crack growth under fatigue loads is known to be influenced by moisture in the surrounding air. Water vapor can significantly accelerate fatigue crack growth and thereby speed the failure of structural components. This effect of water vapor is strongly coupled to the frequency of load fluctuations over a critical range of water vapor pressures. Fatigue crack growth can also be influenced by alloy composition and microstructure, the presence of oxygen, temperature, load ratio (R), material thickness (or thickness in relation to plastic zone size), stress intensity range, and the processes used in preparing the alloys. It is recognized that the interactions among these variables complicate the proper interpretation and extrapolation of experimental data and introduce additional uncertainties with respect to damage-tolerant design and failure analysis.

Under an AFOSR contract (No. F49620-81-K-0004) to Lehigh University, with McDonnell Douglas Research Laboratories participating as subcontractor, a systematic investigation is being conducted of the effects of environmental, mechanical, and metallurgical variables on the fatigue crack growth characteristics of high strength I/M and P/M aluminum alloys. Program objectives and scope, and progress during the second year are summarized.

2.0 Program Objectives and Scope

The program is directed towards (1) the development of a quantitative understanding of the influence of metallurgical variables on the rates and mechanisms of surface reactions of water vapor with I/M and P/M aluminum alloys, and the chemical, metallurgical and mechanical interactions responsible for environmentally assisted fatigue crack growth, and (2) the formulation and evaluation of improved models for predicting crack growth response. It uses the combined fracture mechanics, surface chemistry and materials science approach that has been applied successfully to elucidate environmentally assisted crack growth in steels and titanium alloys, and will capitalize on models that have already been developed (see [1-3] and other references cited therein).

The specific research objectives are to:

(1) Quantify the influences of composition and microstructure (including precipitate type and distribution, impurities, etc.) on chemical reaction kinetics and fatigue crack growth rates and response, with particular emphasis on comparisons between I/M and P/M alloys.

(2) Verify the proposed model [1-3] for a range of aluminum alloys, with different compositions and microstructures, by measuring both fatigue crack growth response as a function of water vapor pressure and frequency, and the appropriate chemical reaction rates.

(3) Modify the proposed model [1-3] to incorporate other significant variables (such as load ratio, waveform, and thickness), and verify the model for a broad range of loading and environmental variables.

(4) Develop a quantitative mechanism for embrittlement and formulate a model for estimating the rates of environmentally assisted fatigue crack growth that incorporates the significant chemical, metallurgical and mechanical variables.

Fracture mechanics techniques, quantitative metallography (including scanning and transmission electron microscopy), and surface analysis techniques (such as Auger electron and x-ray photoelectron spectroscopy) are used.

2219-T851, 7050-T7451 (formerly 7050-T73651) and 7075-T651 aluminum alloys are included in this study to represent 2XXX and 7XXX series I/M alloys that are or may be used in current and advanced Air Force aircraft. Alloy X7091, the most probable 7XXX series P/M alloy to be utilized and to be available in quantity, was selected as the representative 7XXX series P/M alloy. Since no suitable 2XXX series P/M alloy is currently available, a small quantity of P/M alloy is being made to the 2219 alloy composition for use in the third year of this study. These alloys provide a reasonable range of composition and microstructure for evaluation and comparison. Two aging treatments are used on the 7050 (I/M) and X7091 (P/M) alloys to further investigate the influence of temper and microstructure. Results from this study will be compared with available data on other 2XXX and 7XXX alloys to broaden the basis of understanding corrosion fatigue mechanisms.

Adequate numbers of replicate tests will be carried out for selected alloys and test conditions to assess inter- and intra-laboratory variability and to ensure statistical significance of the test results.

This research is being conducted by Lehigh University (LU) and the McDonnell Douglas Research Laboratories (MDRL) as a technical team, with Lehigh serving as the lead laboratory (prime contractor), and is planned for three (3) years. Dr. Robert P. Wei from Lehigh and Dr. Peter S. Pao from MDRL are the principal personnel involved with this program. Dr. Gary W. Simmons of Lehigh is providing support for the surface chemistry portions of the program. Mr. Ming Gao, a Ph.D. candidate in Metallurgy and Materials Engineering, is participating in this program as a Research Assistant.

3.0 Summary of Progress

The program was initiated on 1 January, 1981. During the first year, principal effort was directed to the study of 7050-T7451 (I/M) alloy. Initial qualification tests and characterizations of the 7075-T651 (I/M) and X7091 (P/M) alloys were also conducted. These results were reported in the first annual report of this contract [4].

During this year, the influences of water vapor and of water vapor-oxygen mixtures on the kinetics of fatigue crack growth in ingot-processed 7075-T651 alloy and in powder-processed X7091-T7E69 and X7091-T7E70 alloys were determined. Fractographic examinations of specimens tested in the various environments were also carried out to provide information for identifying the role

of microstructure in environmentally assisted fatigue crack growth. Mechanical properties, texture and microstructural characterizations of the X7091 (I/M) alloys were also made. Progress during the second year is summarized in the following sections.

3.1 Qualification and Microstructural Characterization

Qualification and microstructural characterization of 7050-T7451 and 7075-T651 were made during the first year and have been reported [4]. References to these qualification and characterization results are made for comparison to the X7091 (P/M) alloys.

38 mm by 114 mm (1.5 in. by 4.25 in.) extrusions of X7091-T7E69 and X7091-T7E70 (P/M) alloys were obtained from ALCOA. The T7E69 designation refers to an over-aging treatment of 4 h, while T7E70 refers to over-aging for 14 h. Chemical composition and tensile properties of these extrusions were supplied by ALCOA and are given in Table 1 [5]. Fracture toughness of these extrusions was measured with the use of 24.7 mm (0.97 in.) thick wedge-opening-load (WOL) specimens. For X7091-T7E69, the plane strain fracture toughness, K_{Ic} was determined to be 44.6 MPa-$m^{1/2}$. The measured fracture toughness for X7091-T7E70 of 58.7 MPa-$m^{1/2}$ failed to satisfy the specimen thickness requirement and is not considered to be a valid K_{Ic} measurement. Information on the 7050-T7451 and 7075-T651 (I/M) alloys used in this study are included in Table 1 for comparison [4,6,7].

The crystallographic texture of X7091-T7E70 alloy was determined from the distributions of {200}, {220} and {111} poles

at the surface and mid-thickness planes of the extrusion (see Figs. 1 and 2). The results indicate that the X7091-T7E70 alloy has a $(11\bar{0})[1\bar{1}2]$ type texture. This texture is similar to that observed in the 7050-T7451 alloy plate [4], except that the texture is sharper in the X7091-T7E70 alloy extrusion. Texture determination was not made on the X7091-T7E69 alloy extrusion. It is expected, however, that the texture for the two extrusions would be similar.

Transmission electron micrographs of X7091-T7E70 alloy are shown in Figs. 3 and 4. Figure 3 shows typical grains or subgrains of this alloy, which are on the order of 1 to 3 μm in dimension. The pair of bright-field and dark-field transmission electron micrographs in Fig. 4 show the precipitates in this alloy. The precipitates in the matrix and along the grain boundaries are the equilibrium η ($MgZn_2$) and intermediate η' phases [4,8]. Some coarse precipitates are present at the boundaries, and there appears to be a narrow precipitate free zone adjacent to the grain boundaries. Large constituent particles, unlike the I/M alloys, were not observed in this X7091 (P/M) alloy.

3.2 Kinetics of Fatigue Crack Growth

The kinetics of fatigue crack growth in 7075-T651 (I/M) aluminum alloy and in X7091-T7E69 and X7091-T7E70 (P/M) aluminum alloys at room temperature have been determined, for a frequency of 5 Hz and load ratios R = 0.1 and 0.5. Test environments included vacuum, pure argon, pure oxygen at 266 Pa, and pure water vapor (over a range of pressures from 0.13 to 1330 Pa, or

0.001 to 10 torr). Tests in argon and in oxygen were carried out to provide additional reference data and for comparison. To examine the possible role of oxygen in inhibiting the influence of water vapor on fatigue crack growth, tests were also conducted in oxygen-water vapor binary mixtures. A fixed water vapor partial pressure of 67 Pa (0.5 torr) was selected, while the oxygen partial pressure covered a range from 0.466 to 200 kPa (3.5 to 150 torr). Specific loading and environmental conditions are given in Table 2. Principal results from these tests are summarized separately for the I/M and P/M alloys in the following subsections. Comparisons between the crack growth responses for I/M and P/M alloys are made.

3.2.1 7075-T651 (I/M) Aluminum Alloy

Representative fatigue crack growth data for 7075-T651 (I/M) aluminum alloy tested in vacuum, pure argon and pure oxygen are shown in Fig. 5. Data for tests in water vapor at R = 0.1 and R = 0.5 are shown in Figs. 6 and 7 respectively. The influence of water vapor on fatigue crack growth in this I/M alloy, at R = 0.1, is shown explicitly in Fig. 8 for two ΔK levels.

The results shown in Figs. 5, 6 and 8 indicate that the crack growth rates in vacuum and in argon are faster than those observed in pure water vapor at the lowest vapor pressures (1.3 and 2 Pa). The rates are also faster than those observed in oxygen. The crack growth rate in oxygen, however, are comparable to those in water vapor at 1.3 and 2 Pa. The reasons for the faster growth rates in vacuum and in argon are not yet understood. Fractographic results to be described later, however, do

indicate a difference in the micromechanism for crack growth in vacuum and in argon from that in oxygen and low pressure water vapor. For the interpretation of data in terms of the model for transport controlled crack growth [1-3], it appears appropriate to used the data in pure oxygen as the reference rates, i.e., $(da/dN)_r$.

From Fig. 8 it is seen that at low water vapor pressures, fatigue crack growth rates are strongly dependent on pressure, and conform to the model for transport controlled crack growth as indicated by the solid lines in the figure. The "saturation" water vapor pressure is estimated to be about 4.7 Pa [2,3]. Above the saturation pressure, crack growth rates are essentially independent of water vapor pressure up to 100 Pa.

At higher vapor pressures (above 600 Pa) and in liquid water, the crack growth rates exceeded those of the "saturation" level (see Fig. 8). The rates at 1.3 kPa and in distilled water are about twice higher than the "low pressure" saturation rates. The observed further increase in growth rate is consistent with the results reported by Dicus [10] for 7475-T651 aluminum alloy. Taken together, these results indicate that there might be a second transition in crack growth rate with water vapor pressure. The cause for this transition is being investigated in relation to the surface reaction kinetics.

To investigate the possible inhibiting effects of oxygen on the enhancement of fatigue crack growth by water vapor, crack growth measurements were made in binary mixtures of water vapor and oxygen. The ratio of partial pressures of water vapor to

oxygen was varied from 1:7 to 1:300, while the water vapor pressure was maintained constant at 67 Pa. A test was also carried out in air, at 42 pct relative humidity, to provide for comparison.

No inhibiting effect of oxygen was observed under these test conditions (see Fig. 9). These results are not in agreement with model predictions [3], and are at variance with convincing evidence in support of the inhibition of crack growth by oxygen [10,11], at least for sustained loading. Plausible explanations for the observed response and additional studies are considered in Section 3.2.3.

3.2.2 X7091-T7E69 and X7091-T7E70 (P/M) Aluminum Alloys

Wedge-opening-load (WOL) specimens, with LT orientation, were used to determine the kinetics of fatigue crack growth in the X7091 (P/M) alloys. In the early tests, it was found that the fatigue crack deviated by more than 10 degrees from the plane of symmetry (or the intended crack plane) in about 50 pct of the cases. This large deviation rendered the test data invalid [12]. An example of such a deviation is shown in Fig. 10a, which is commonly observed in powder processed aluminum alloy specimens tested in the LT orientation.

To alleviate this problem, face grooving of the specimens was employed. A face groove, with depth equal to 5 or 10 pct of the specimen thickness, was introduced into each face of the test specimen along the desired crack growth direction. The effectiveness of face grooving in confining the fatigue crack to the plane of symmetry is illustrated in Fig. 10b for the case of

a 5 pct deep groove. Fatigue data reported herein were obtained either from the face grooved specimens or from the ungrooved specimens that were deemed to be acceptable [12].

Representative fatigue crack growth data for X7091-T7E69 and X7091-T7E70 alloys tested in vacuum and in water vapor are shown in Fig. 11. Composite trend lines for these alloys are shown in Fig. 12. Comparison of Figs. 12a and 12b shows that fatigue crack growth rates are comparable for the X7091-T7E69 and X7091-T7E70 alloys, although the latter alloy was overaged for a longer period of time (14 h vs. 4 h). Depending on the ΔK level, enhancement of fatigue crack growth rates by water vapor is as much as a factor of 2 over that observed in vacuum.

The influence of water vapor pressure on the rate of fatigue crack growth in these alloys is shown more explicitly in Fig. 13 at three ΔK levels. Test data from both X7091-T7E69 and X7091-T7E70 alloys have been combined in this figure. It is seen, from Fig. 13, that fatigue crack growth rate started to increase when the water vapor pressure exceeded a threshold level of about 0.13 Pa. Above this threshold pressure, crack growth rate increased with increasing vapor pressure, and reached a maximum and then remained constant above a "saturation" pressure. The observed response is again consistent with the model for transport controlled fatigue crack growth [2,3]. The saturation pressure for the X7091 (I/M) alloys is estimated to be about 0.67 Pa, and the range of pressure over which fatigue crack growth rates remained essentially unchanged in this study extended from about 0.67 to 66.7 Pa.

Tests in mixtures of water vapor and oxygen were also carried out on X7091-T7E70 (P/M) alloy, with a fixed water vapor partial pressure of 67 Pa and water vapor to oxygen partial pressure ratios from 1:21 to 1:300. The test results are shown in Fig. 14. Again, in agreement with similar results on the 7075-T651 (I/M) alloy, there was no apparent inhibiting effect of oxygen under these test conditions. The implications of these results are also considered in Section 3.2.3.

3.2.3 Comparison between I/M and P/M Alloys and Discussions

Because the various portions of the fatigue crack growth experiments were carried out at two different laboratories (Lehigh and MDRL), it is important to assess inter-laboratory variability before comparison of data are made. Figure 15 shows the results of replicate fatigue crack growth tests in vacuum on X7091-T7E70 (P/M) alloy conducted at the two laboratories. Reproducibility of results appears to be very good (statistical evaluation is being carried out to confirm this observation [15,16]). An additional indication of reproducibility can be seen by comparing the test results for water vapor (obtained at MDRL) with those in the water vapor-oxygen mixture (obtained at Lehigh) in Fig. 14. Preliminary estimates suggest that reproducibility of data is within 10 pct between the two laboratories and within each laboratory. Based on these comparisons and estimates, it is reasonable to make direct and quantitative comparisons between the various data sets.

Comparison of Figs. 8 and 13 shows that the crack growth response of X7091 (P/M) alloys closely resembles that of 7075-

moisture, as measured by the ratio between the "saturation" growth rate and the "reference" rate, however, is greater than that of the X7091 alloys. The difference in saturation pressures, at a given test frequency, between the alloys (4.7 vs. 0.67 Pa) cannot be fully accounted for by their differences in yield strength [2,3,13]. This difference may be attributed to differences in fracture surface roughness (see Section 3.3), which is reflected in the values of β^*/α shown in Table 3.

A comparison between the crack growth kinetics for X7091-T7E69 (P/M) and 7050-T7451 (I/M) alloys, which contain similar major alloying elements, is shown in Fig. 16. It is seen that fatigue crack growth rates are faster in the P/M alloy for both water vapor and vacuum, particularly in the lower ΔK region. The faster growth rates in the powder processed X7091-T7E69 alloy are attributed to its finer grain/subgrain size, which reduces slip reversibility and produces less zig-zag in crack path. At high ΔK, the effect of grain size diminishes and the fatigue crack growth rates in X7091-T7E69 alloy become comparable to those in 7050-T7451.

The apparent absence of inhibition of crack growth by oxygen in the binary water vapor-oxygen mixtures for both the I/M and P/M alloys is puzzling. An indication of this behavior was seen in the data of Bradshaw and Wheeler [14], particularly at the lower ΔK levels. A plausible explanation is that water vapor condenses at the crack tip and thereby effectively shields the crack tip from exposure to oxygen. This possibility needs to be tested by examining the crack growth response at lower water

vapor partial pressures (that is, well below 67 Pa used in the present experiments) over the same range of partial pressure ratios. These tests are in progress. Another possibility is that the kinetics of reactions of oxygen and water vapor with the 7XXX series alloys are considerably different from those of the 2XXX series alloys [1]. This is not likely to be the case, but is to be resolved by the ongoing surface chemistry experiments.

3.3 Fractographic Analyses

To assist in understanding the role of metallurgical and chemical variables on environmentally assisted fatigue crack growth, fractographic analyses were performed on fatigue fracture surfaces of 7075-T651 (I/M) and X7091 (P/M) alloys. Systematic observations were made of the changes in fracture surface morphology as a function of water vapor pressure to assist in elucidating the mechanism for embrittlement. This information, along with fractographic data obtained from specimens tested in inert environments, serves as a basis for the formulation of a quantitative model for estimating the rates of environmentally assisted fatigue, which would incorporate the significant chemical, metallurgical and mechanical variables. Fractographic results from the 7075-T651 (I/M) and X7091 (P/M) alloys are presented and discussed separately.

3.3.1 7075-T651 (I/M) Alloy

Representative scanning electron (SEM) microfractographs taken from specimens tested in vacuum, pure oxygen and pure water vapor are shown in Figs. 17 to 28. Fractographs and stereo pairs from mating fracture surfaces were obtained to provide more detailed information on the fracture processes (see Figs. 18, 19, 20, 22, 27 and 28). Because the effect of water vapor pressure on fracture surface morphology is of special interest, particularly in the low pressure region where the crack growth rates are controlled by gas transport, microfractographs representing five different water vapor pressures (that is, 1.3, 2.7, 4.6, 67, and 670 Pa) have been included (see Figs. 23 to 26).

Vacuum

Comparisons of Figs. 17 to 20 with Figs. 21 to 28 show that the morphology of fracture surface produced in vacuum is clearly different from those produced in pure oxygen and in water vapor. Figure 17 shows that the fracture surface is composed of regions that are associated with (constituent) particles and regions that are relatively featureless. More detailed nature of the fracture surfaces may be seen in the SEM microfractographs and stereo pairs of the mating surfaces (Figs. 18 to 20).

A close match between mating surfaces is seen. Holes on one surface are closely matched to particles or protrusions on the other surface. Every ridge on the one surface has a corresponding valley on the other. This correspondence indicates the "brittle nature" of fatigue cracking in 7075-T651 as compared to the more "ductile", void coalescence mode found in over-load

fracture; where ridges correspond to ridges, and valleys to valleys. Slip steps are more pronounced on one surface than the other (Figs. 18 to 20). The implications of these observations are not clear and are being examined.

Because of the differences in fracture surface morpholgy and in crack growth rates between specimens tested in vacuum and those tested in oxygen and at the lowest water vapor pressure, there is reason to believe that the mechanism of fatigue cracking in vacuum is different. The reason for this difference is unclear, and may be associated with either the influence of surface oxides on slip (i.e., deformation) or local heating at the crack tip. It appears, therefore, that the fatigue crack growth rates in vacuum should not be used as a reference in evaluating the models for environmentally assisted crack growth.

Oxygen

Since the crack growth rates in pure oxygen (at 266 Pa) are comparable to those in water vapor at the lowest test pressure of 1.3 Pa, it is important to compare the fracture surface morphology between these two cases. SEM microfractographs for the specimen tested in 267 Pa pure oxygen are shown in Figs. 21 and 22.

It can be seen that the fracture surface morphology of the specimen tested in oxygen is nearly identical to that of the specimen tested in 1.3 Pa water vapor; (compare Figs. 21 and 23). The surface is composed of (1) dense clusters of dimples that are associated with large constituent particles, (2) regions of extensive plastic deformation (ductile tearing), and (3) a small amount of flat featureless facets. Energy dispersive x-ray

(EDAX) analyses showed that these particles are rich in iron and in copper.

Because of the similarity in fracture surface morphology hence, micromechanism of cracking in crack growth rates for these two environments (pure oxygen and 1.3 Pa water vapor), it is reasonable to use pure oxygen as the reference environment for analyzing fatigue crack growth data in water vapor. The observed micromechanism for crack growth is identified with that for "pure" mechanical fatigue in this alloy.

Water Vapor

The changes in surface morphology as a function of water vapor pressure are illustrated in Figs. 23 to 26. Figure 23 shows representative microfractographs taken from a specimen that had been tested in water vapor at 1.3 and 670 Pa. The micrographs clearly show two regions with completely different fracture surface morphology.

The fracture surface produced in 670 Pa water vapor (region A in Fig. 23a, and Fig. 23b) is flat and appears to be brittle. The brittle nature of cracking in water vapor at the higher pressures is confirmed by stereo pairs of SEM microfractographs obtained from mating fracture surfaces of 7075-T651 alloy tested in 133 Pa water vapor (Figs. 27 and 28). Brittle striations or slip steps are clearly discernible in each of the mating surfaces, and the various microscopic facets are closely keyed with each other across the crack plane. The surface produced in 1.3 Pa water vapor (region B in Fig. 23a, and Fig. 23c), on the

other hand, appears to be rougher and more "ductile"; exhibiting extensive amounts of ductile tearing and dimpled rupture.

This marked contrast in microscopic fracture appearance suggests the operation of at least two different micromechanisms, and provides a basis for the interpretation and correlation of fractographic data. As an initial effort, one may choose to identify the fracture morphology for 670 Pa water vapor (Fig. 23b) with the micromechanism for "pure" corrosion fatigue. The morphology shown by the tests in 1.3 Pa water vapor (Fig. 23c) and in pure oxygen is identified with "pure" mechanical fatigue.

Based on these premises, it can be seen clearly from Figs. 23 to 26 that the fraction of fracture surface created by "corrosion fatigue" increased rapidly as the water vapor pressure increased from 1.3 to 67 Pa. The fracture surface morphology of specimens tested at pressures higher than 4.7 Pa was essentially identical to that of specimens tested at 670 Pa; i.e., 100 pct by corrosion fatigue.

More quantitative measurements of the areal fraction of each component on the fracture surface as a function of water vapor pressure are being made. This information, coupled with the data on crack growth kinetics would provide further insight and advance the understanding of the micromechanism of environmentally assisted fatigue crack. It would also provide experimental support for the proposed modification to the superposition model for fatigue crack growth (see Section 3.4).

3.3.2 X7091 (P/M) Alloy

Representative SEM microfractographs from X7091-T7E69 alloy tested in vacuum and in 13.3 Pa water vapor, at ΔK of 11 MPa-$m^{1/2}$, are compared in Fig. 29. Representative SEM microfractographs from X7091-T7E70 alloy tested in pure oxygen at 267 Pa, also at ΔK of 11 MPa-$m^{1/2}$, are shown in Fig. 30. These microfractographs indicate that the fracture path in all three environments is primarily transgranular and is typical of high strength aluminum alloys fractured in fatigue. No clearly discernible fatigue striations can be found for any of the test environments.

The morphology of fracture surfaces for specimens tested in water vapor is different from that for specimens tested in vacuum and in oxygen. Fracture surfaces in vacuum and in oxygen exhibited finer features and more ductile tearing than those in water vapor. Regions showing the presence of constituent particles were also observed on the fracture surfaces exposed in oxygen, although the density and size of these particles are much smaller than those in the ingot-processed 7075-T651 alloy. Fracture surfaces of specimens tested in water vapor are characterized by many flat patches and smaller areas of ductile tearing. Some slip steps are discernible in the flat patches. This type of fracture surface morphology is a good indication that the fatigue crack had propagated through previously "embrittled" zones, as envisioned in the proposed model for environmentally assisted fatigue crack growth.

3.3.3 Comparison between I/M and P/M Alloys

Comparisons of the SEM microfractographs for the I/M 7075 and P/M X7091 alloys, for the respective environments, show that, overall, the micromechanisms for fatigue crack growth are essentially similar. The constituent particles are smaller and far fewer in the powder processed alloy. Being much finer in grain (and subgrain) size, the detailed fracture surface features are much more difficult to discern in the P/M alloys, vis-à-vis, the I/M alloy.

A more direct comparison of the fracture surface morphology of powder-processed 7091-T7E69 and ingot-processed 7050-T7451 alloys is given in Fig. 31. Both specimens were tested in water vapor and the SEM microfractographs were taken from regions of fracture surfaces that correspond to a ΔK of 11 MPa-$m^{1/2}$.

Since fatigue crack propagated primarily along crystallographic planes in both P/M 7091 and I/M 7050 alloys, the crack path (hence, the fracture surface morphology) would be influenced strongly by the orientation and the size of the grains encountered by the crack. During fatigue, a crack that followed one set of slip bands in one grain (or subgrain) would be forced to continue on another set of slip bands and change orientation when it encountered the neighboring grain or subgrain boundary, thus forming a zig-zag crack path.

In the I/M 7050-T7451 alloy (Fig. 31b), this zig-zag crack pattern or macroscopic fracture surface roughness is much more pronounced, when compared to the X7091-T7E69 (P/M) alloy, because of the much larger grain (or subgrain) size of the I/M alloy. As

the crack follows the zig-zag path, it deviates locally from the plane of symmetry. As a result, the effective stress intensity factor at the crack tip is slightly reduced and thereby lowers the corresponding crack growth rate. The more pronounced zig-zag crack path in the large-grain I/M 7050-T7451 alloy may be partially responsible for the lower observed fatigue crack growth rates as compared to the X7091-T7E69 (P/M) alloy.

More detailed fractographic examinations of the X7091 (P/M) alloy are in progress. Further comparisons of I/M and P/M alloys will be made to aid in understanding the role of metallurgical variables on environmentally assisted fatigue crack growth.

3.4 Modeling

A modification of the superposition model [17] for corrosion fatigue has been made to give explicit recognition to the fact that mechanical fatigue and corrosion fatigue can proceed by different micromechanisms and occur concurrently or in parallel. The modified model provides a firmer and more consistent basis for the interpretation of fractographic results, but is otherwise fully consistent with (that is, does not invalidate) the transport and surface reaction controlled models for fatigue crack growth [2,3,13].

In the original formulation, crack growth rate was assumed to be the sum of three terms [17]:

$$(da/dN)_e = (da/dN)_r + (da/dN)_{cf} + (da/dN)_{scc} \qquad (1)$$

The first two terms represent the contributions of mechanical fatigue and cycle-dependent corrosion fatigue, and the last term,

the contribution of sustained-load growth or SCC. Because the first two processes occur concurrently or in parallel, simple summation of rates is not appropriate even though Eqn. (1) correctly represents the experimental data. The addition of the third term is appropriate, since SCC contribution is considered to be sequential. But, because SCC contribution is not important to the consideration of aluminum alloys in the LT and TL orientations, this term is not included in the subsequent discussions.

To give recognition to the concurrent processes, Eqn. (1) is rewritten into the following form:

$$(da/dN)_e = (da/dN)_r\ (1 - \phi) + (da/dN)^*_{cf,s}\ \phi \qquad (2)$$

$(da/dN)_r$ is the mechanical fatigue rate, $(da/dN)^*_{cf,s}$ is the "pure" corrosion fatigue rate, and ϕ is the fractional area of crack that is undergoing pure corrosion fatigue. In the limit, for $\phi = 0$ or for test in an inert environment, $(da/dN)_e = (da/dN)_r$, which corresponds to pure fatigue. For $\phi = 1$, corresponding to saturation [2,3], $(da/dN)_e = (da/dN)_{e,s} = (da/dN)^*_{cf,s}$ or the pure corrosion fatigue rate. By rearranging Eqn. (2) and recognizing the correspondence between ϕ and θ (the fractional surface coverage [2,3]), it is clear that the modified model is identical to the original version [17], where $[(da/dN)^*_{cf,s} - (da/dN)_r] = (da/dN)_{cf,s}$.

$$\text{Modified:}\quad (da/dN)_e = (da/dN)_r + [(da/dN)^*_{cf,s} - (da/dN)_r]\phi \qquad (3)$$

$$\text{Original:}\quad (da/dN)_e = (da/dN)_r + (da/dN)_{cf}$$

$$= (da/dN)_r + (da/dN)_{cf,s}\ \theta \qquad (4)$$

The implications of the modified model are that the partitioning of hydrogen to the various microstructural sites would not be uniform. The fractional area of fracture surface (ϕ) produced by pure corrosion fatigue would be equal to θ, and would conform to one of the models for corrosion fatigue [2,3]. Statistically reliable experimental verification is difficult. Preliminary indication deduced from fractographs, such as those shown in Figs. 23-26, tends to support this modified model (see Fig. 32). Additional crack growth experiments and more detailed fractographic analyses are planned for the third year of this program to provide further quantitative support.

4.0 Summary

The influence of water vapor on the kinetics of fatigue crack growth in 7075-T651 (I/M) alloy and X7091-T7E69 and X7091-T7E70 (P/M) alloys has been systematically determined. The possible influence of oxygen in inhibiting the enhancement of fatigue crack growth by water vapor was also examined. Detailed fractographic analyses were performed on these alloys to provide information on the role of metallurgical variables on fatigue crack growth.

Fatigue crack growth response of the X7091 (P/M) alloys in water vapor is similar to that of 7075-T651 (I/M) alloy and agrees well quantitatively with the transport-controlled model for fatigue crack growth. Fatigue crack growth rates in the X7091 (P/M) alloys are higher than those in the 7050-T7451 (I/M) alloy over the low and intermediate ΔK range. The higher growth

rates may be explained by the effects of grain size on slip reversal and on fracture surface roughness.

Fractographic examinations suggested that the crack growth mechanism in oxygen and at low water vapor pressures may be different from that in vacuum for these aluminum alloys. The fracture surface morphology varied continuously as water vapor pressure was increased. At low water vapor pressures and in oxygen, fracture surfaces of 7075-T651 alloy contained dense clusters of dimples, associated with large constituent particles, and regions of extensive deformation. At the higher water vapor pressures, the fracture surfaces were essentially brittle. Stereographic analyses of the mating surfaces of 7075-T651 alloy indicate the close match between the surfaces and the limited extent of (ductile) deformation on the gross scale. Further analyses and comparisons between the I/M and P/M alloys are in progress.

For a water vapor partial pressure of 67 Pa (with load ratio R = 0.1), oxygen appeared to exert no inhibiting effect on fatigue crack growth in the 7075-T651 and X7091 aluminum alloys for oxygen-water vapor partial pressure ratios from 4 to 300. This apparent disagreement with expectation and model prediction is being examined.

A modification of the superposition model for corrosion fatigue has been made to give explicit recognition to the fact that mechanical fatigue and corrosion fatigue can proceed by different micromechanisms and in parallel. Preliminary analysis of

fractographic data from this study tends to support this modification. Additional experimental support is to be developed during the next year.

5.0 Planned Research

The planned research for the third year of this program essentially conforms to the original proposal. The specific items include the following:

- o Examination of the influence of aging treatment on the kinetics of fatigue crack growth in 7050 (I/M) alloy.
- o Determination of the influence of water vapor on fatigue crack growth in a 2XXX series (P/M) alloy. (A P/M alloy, conforming to the 2219 alloy composition, has been ordered. Delivery is expected in April. Data from this alloy will be used for comparison with 2219-T851 and with the 7XXX series I/M and P/M alloys.)
- o Measurements of the kinetics of surface reactions of water vapor and oxygen with the 7XXX series I/M and P/M alloys for correlations with crack growth kinetics and for modeling environmentally assisted fatigue crack growth.
- o Exploratory investigations of the influences of temperature and specimen thickness on crack growth response.
- o Fractographic and metallurgical analyses in support of the aforementioned studies.

6.0 Acknowledgement

The X7091-T7E69 (P/M) and 7050-W alloys were provided to this program by ALCOA through the courtesy of the ALCOA Foundation. The kind assistance of Phil Bretz, Robert Bucci and Walt Cebulak of ALCOA, with material procurement and in providing material property data, is gratefully acknowledged.

7.0 REFERENCES

1. R. P. Wei, P. S. Pao, R. G. Hart, T. W. Weir, and G. W. Simmons, Met. Trans. A, 11A, 151-158 (Jan., 1980).

2. T. W. Weir, R. G. Hart, G. W. Simmons, and R. P. Wei, Scripta Met., 14, 357-364 (1980).

3. R. P. Wei and G. W. Simmons, "Surface Reactions and Fatigue Crack Growth", Proceedings of 27th Sagamore Army Materials Research Conference on Fatigue - Environment and Temperature Effects, Bolton Landing, NY, July 14-18, 1980, to be published.

4. R. P. Wei and P. S. Pao, "Mechanisms of Corrosion Fatigue in High Strength I/M and P/M Aluminum Alloys", Air Force Office of Scientific Research, Technical Report No. 1 (First Annual Report), January 1982.

5. ALCOA Test Data on X7091-T7E69 alloy (Lot G86176-A1) and X7091-T7E70 alloy (Lot G86515-A1).

6. "Wrought P/M Alloys - A Balance of Properties For Demanding Aerospace Application", ALCOA, p. 4.

7. "Aluminum Standards and Data", Aluminum Assoc., Inc., pp. 15 and 111 (1979).

8. J. Gjønnes and Chr. J. Simensen, Acta Metallurgica, 18, 881-890, 1970.

9. Dicus, Dennis L., NASA Technical Memorandum 84477, May 1982.

10. M. O. Speidel, in The Theory of Stress Corrosion Cracking in Alloys, ed. J. C.Scully, NATO, Brussels, 289 (1971).

11. R. P. Wei, in Hydrogen Effects in Metals, I. M. Bernstein and Anthony W. Thompson, eds., The Metallurgical Society of AIME, Warrendale, PA 15086, 677-690 (1981).

12. ASTM E647-81, Standard Test Method for Constant-Load-Amplitude Fatigue Crack Growth Rates Above 10^{-8} m/cycle.

13. True-Twa Shih and R. P. Wei, "The Effects of Load Ratio on Environmentally Assisted Fatigue Crack Growth", to be published in Engineering Fracture Mechanics, 1983.

14. F. J. Bradshaw and C. Wheeler, Intl. J. Fract. Mech., 5, 255 (1969).

15. Mandel, J., Standardization News, STDNA, 5, No. 3, 17, (1977).

16. J. T. Fong and N. E. Dowling, in Fatigue Crack Growth Measurements and Data Analysis, S. J. Hudak, Jr. and R. Bucci, eds., ASTM STP 738, 171 (1981).

17. R. P. Wei, in Fatigue Mechanisms, Proceedings of an ASTM-NBS-NSF Symposium, Kansas City, MO, May 1978, J. T. Fong, ed., ASTM STP 675, American Society for Testing and Materials, 816-840 (1979).

18. S. J. Gao, G. W. Simmons and R. P. Wei, "Fatigue Crack Growth and Surface Reactions in Titanium Alloys Exposed to Water Vapor", 1983, to be published.

19. R. Brazill, G. W. Simmons, and R. P. Wei, J. Eng. Mater. Techn., 1979, vol. 101, p. 199.

8.0 Degrees, Presentations and Publications

Degrees Granted

True-Hwa Shih, M. S. in Applied Mechanic, Lehigh University, Bethlehem, Pa, 1981.

Publications

True-Hwa Shih and R. P. Wei, "The Effects of Load Ratio on Environmentally Assisted Fatigue Crack Growth", to be published in J. Eng. Fract. Mech., 1983.

Presentations

"Reconsideration of the Superposition Model For Environmentally Assisted Fatigue Crack Growth", R. P. Wei and M. Gao, presentation at the 1983 TMS-AIME Annual Meeting, Atlanta, GA, March 7, 1983.

"Influence of Water Vapor on Fatigue Crack Growth in 7075-T651 Aluminum Alloy: Kinetics and Fracture Morphology", M. Gao, P. S. Pao and R. P. Wei, presentation at the 1983 TMS-AIME Annual Meeting, Atlanta, GA, March 7, 1983.

"Environmentally Assisted Fatigue Crack Growth in I/M and P/M Aluminum Alloys", R. P. Wei, P. S. Pao and M. Gao, presentation at the 1983 TMS-AIME Annual Meeting, Atlanta, GA, March 7, 1983.

TABLE 1

Chemical Composition and Mechanical Properties
of X7091, 7050, and 7075 Aluminum Alloys [4-7]

(a) Chemical composition (wt pct)

Alloy	Zn	Mg	Cu	Zr	Cr	Mn	Co	Ti	Fe	Si	O	Al
P/M X7091	5.6-6.9	2.0-3.0	1.1-1.8				0.3-0.5		0.15 (Max)	0.12 (Max)	0.2-0.5	Bal
I/M 7050	5.95	2.04	2.41	0.1	0.018	0.016		0.041	0.1	0.07		Bal
I/M 7075	5.1-6.1	2.1-2.9	1.2-2.0		0.18-0.28	0.3		0.2	0.5	0.4		Bal

(b) Mechanical properties

Alloy	Yield Strength MPa(ksi)	Yield Strength MPa(ksi)	Elongation pct	K_{Ic} MPa$\sqrt{m}$ ksi$\sqrt{in.}$
P/M X7091-T7E69	563(81.7)	622(90.2)	11.5	47.9(43.5)
P/M X7091-T7E70	508(73.7)	566(82.1)	14.0	58.7(53.4)*
I/M 7050-T7451	456(66.2)	515(74.8)	14.2	42.0(38.2)*
I/M 7075-T651	469(68)	538(78)	7.0	29.7(27.0)

*Fracture toughness does not satisfy plane strain criterion.

TABLE 2

Test Matrix

Purpose	Environmental Conditions	X7091-T7E69 R = 0.1	X7091-T7E70 R = 0.1	7075-T651 R = 0.1	7075-T651 R = 0.5
Reference	Vacuum (Pa)	$< 10^{-6}$	$< 10^{-6}$	$< 10^{-6}$	
	Argon (Pa)			1.3×10^{3}	
	Pure oxygen (Pa)			667 Pa	
Effect of Water Vapor Pressure	P_{H_2O} (Pa)	0.67	0.13	1.3*	
			0.27	2.0	
			1.3	2.7	
		6.7		4.7	
		14.7	13.3	13.3	13.3
		67	67	67	67
				133	
				333	
				667	
				1330*	
				Distilled water	
Effect of Oxygen P_{H_2O} = 67 Pa	P_{O_2}/P_{H_2O}		4	7	
			21	22	
			63		
			133		
			300	300	
	Humid Air			42% R.H.	

*Tests were only performed at two stress intensity levels: 11.6 and 15.4 MPa$\sqrt{m}$.

TABLE 3

The Empirical Constant β^*/α for Different Material and Environment Combinations

MATERIAL	ENVIRONMENT	β^*/α	REFERENCES
7075-T651	Water Vapor	2.3	This Study
X7091-T7E70	Water Vapor	14	This Study
2219-T851	Water Vapor	3.8	[1,13]
Ti-6Al-4V	Water Vapor	3.7	[18]
2-1/4Cr-1Mo (A542, Class 2)	Hydrogen Sulfide	3.2	[19]

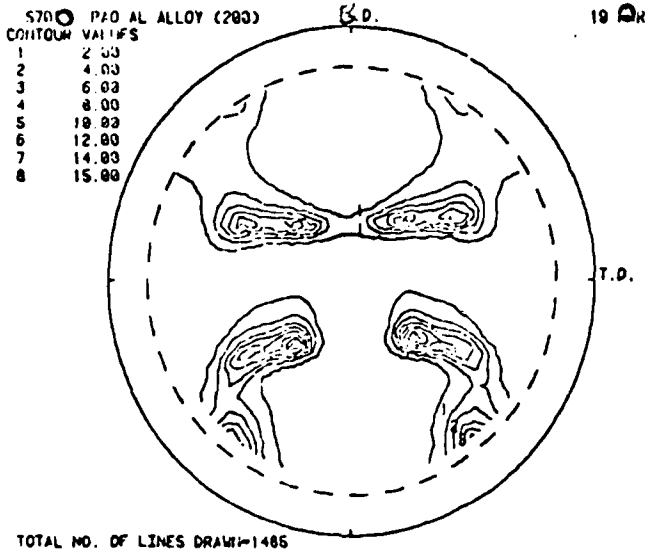

(a) (200) pole

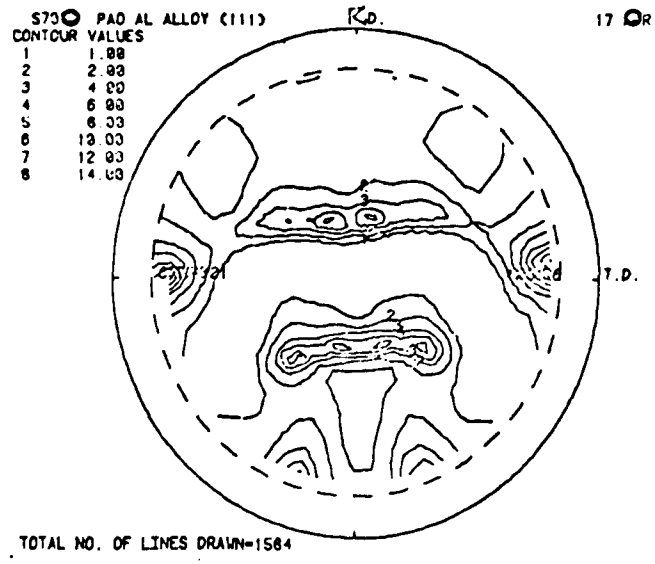

(c) (111) pole

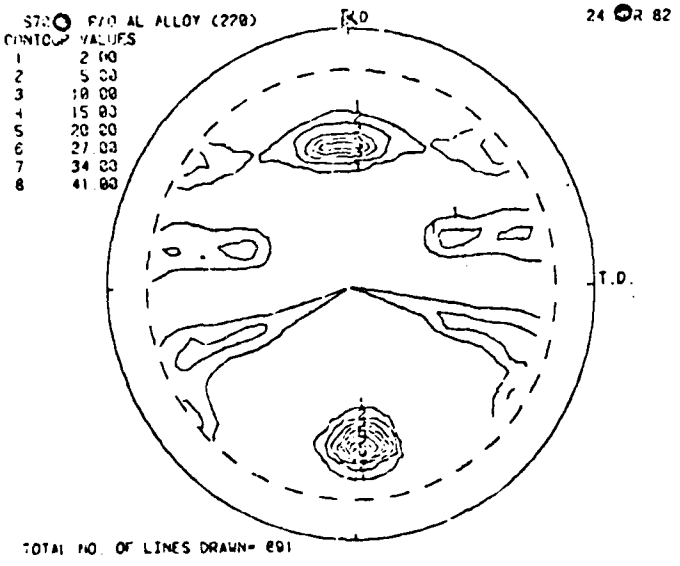

(b) (220) pole

Fig 1: Pole figures for the rolling plane of P/M 7091-T7E70 plate taken at the plate surface: (a) (200), (b) (220), and (c) (111).

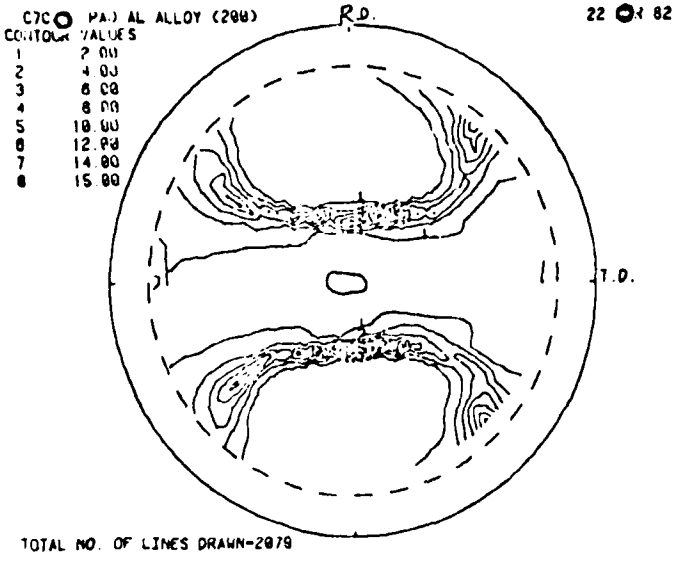

(a) (200) pole

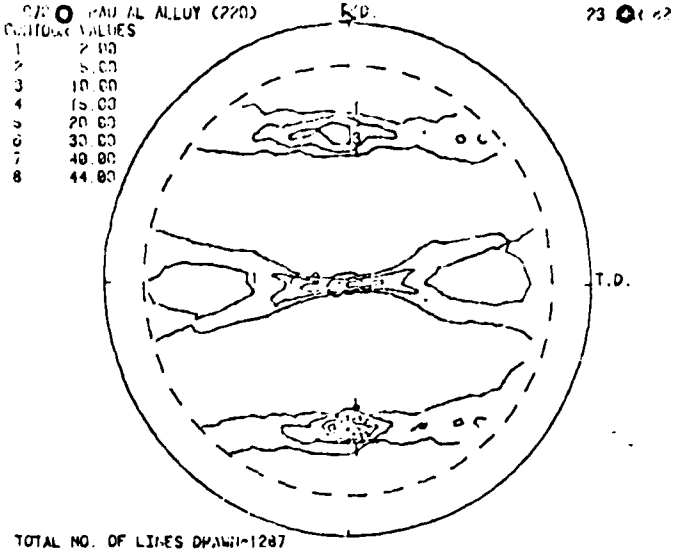

(b) (220) pole

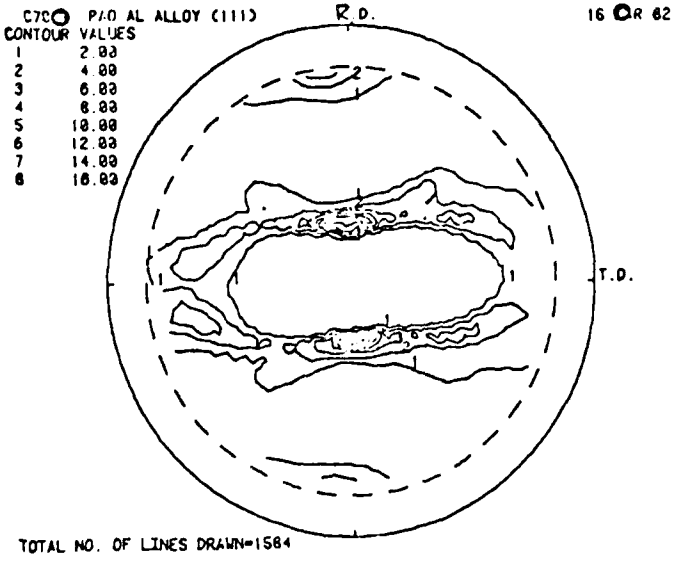

(c) (111) pole

Fig 2: Pole figures for the rolling plane of P/M 7091-T7E70 plate taken at the mid-thickness plane of the plate: (a) (200), (b) (220), and (c) (111).

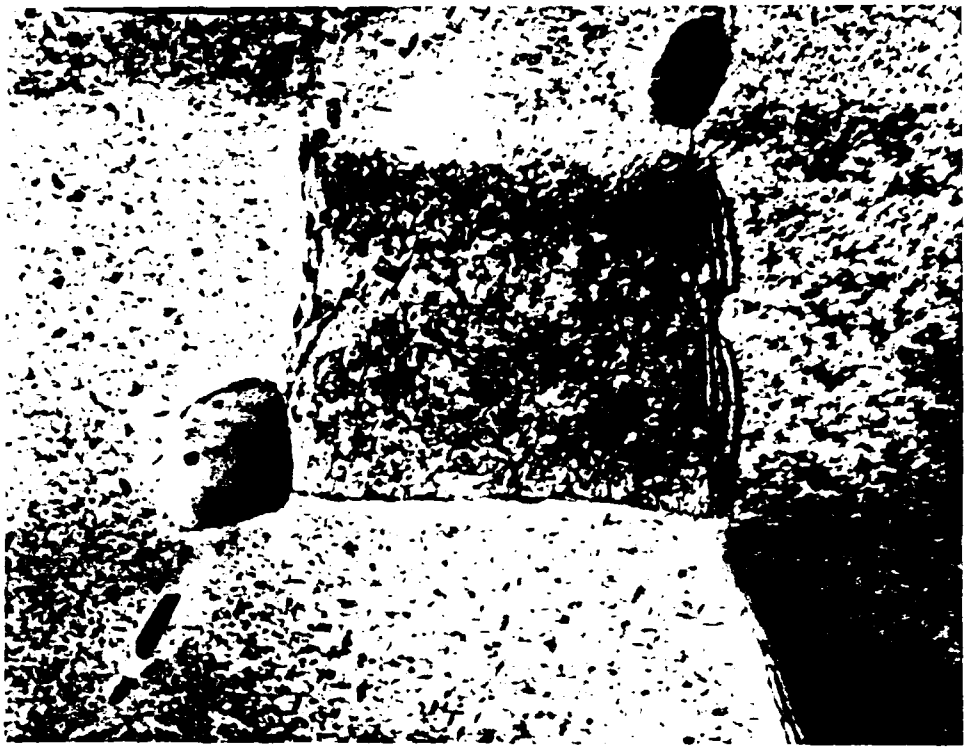

Fig. 3: Transmission electron micrograph of P/M 7091-T7E70. (110,000 X)

(a)

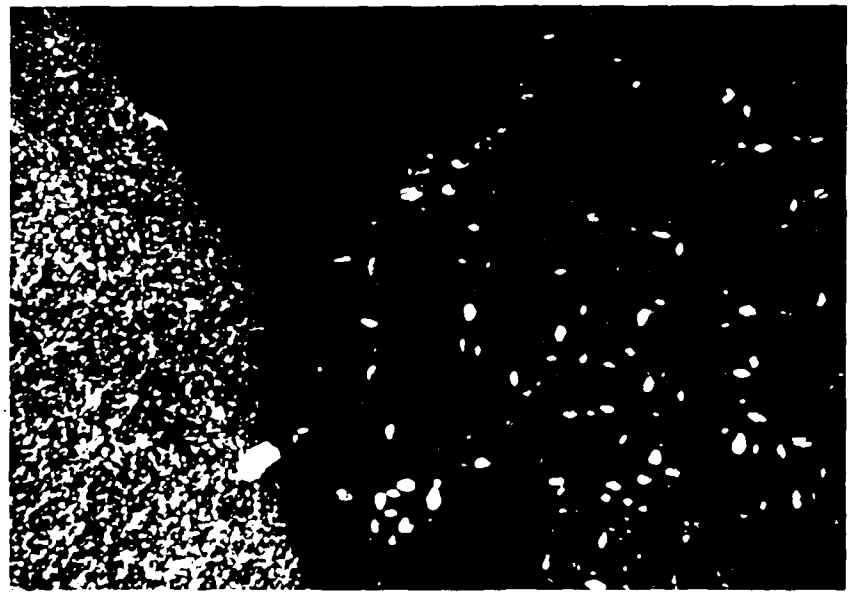

(b)

Fig. 4: Transmission electron micrographs of P/M 7091-T7E70: (a) bright field, and (b) dark field images. (85,000 X)

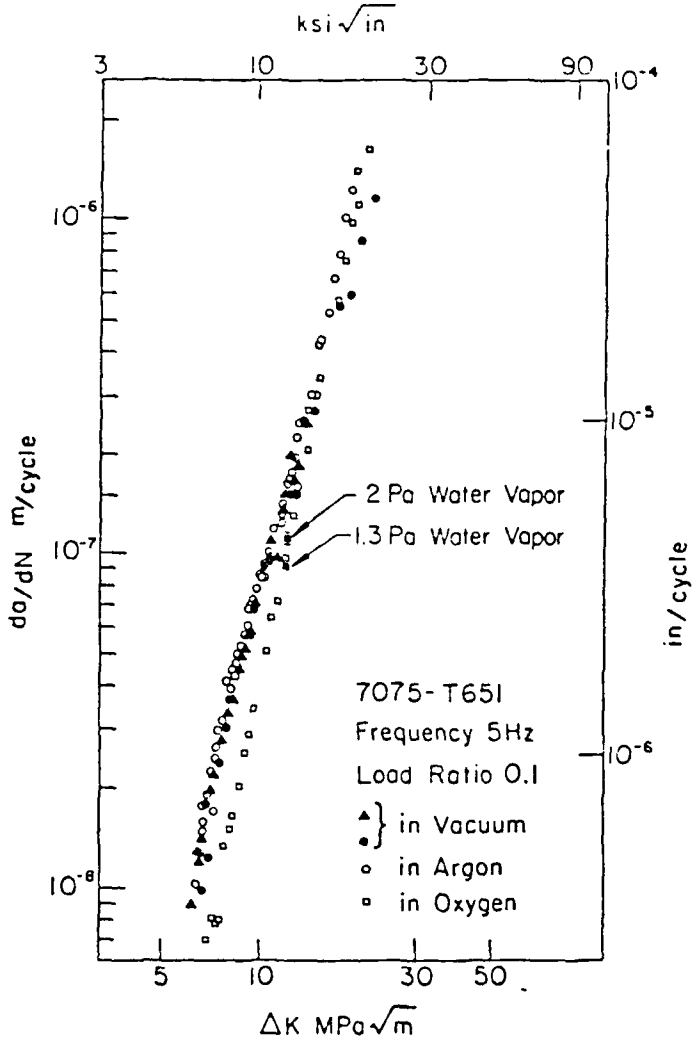

Fig. 5: Comparison of the kinetics of fatigue crack growth in I/M 7075-T651 in vacuum, pure argon and pure oxygen.

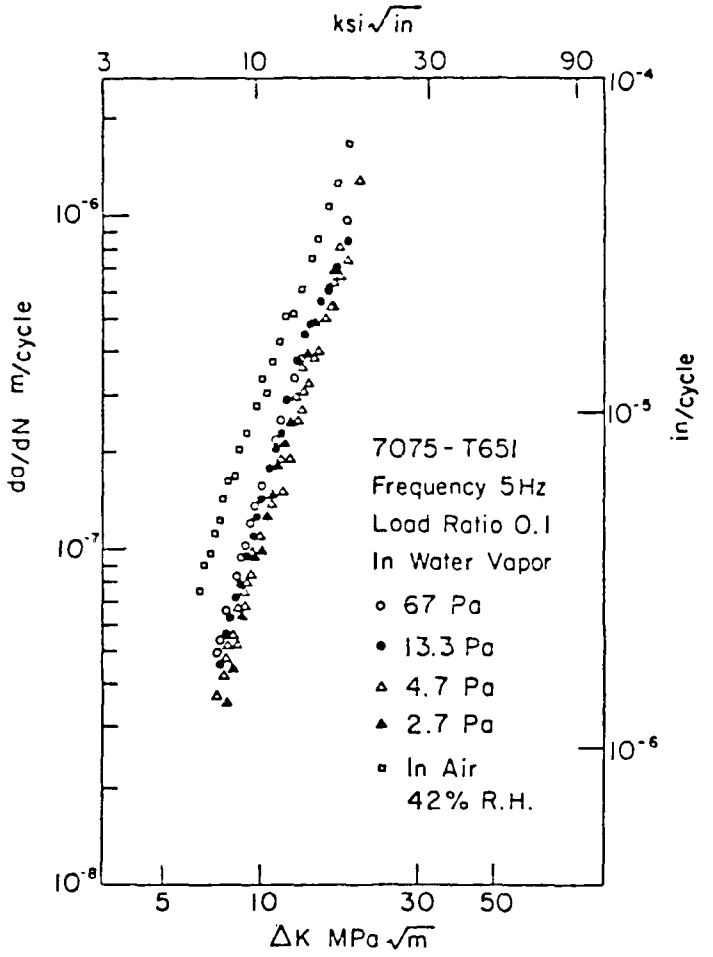

Fig. 6: Effect of water vapor pressure on fatigue crack growth kinetics for I/M 7075-T651 (f = 5 Hz, R = 0.1).

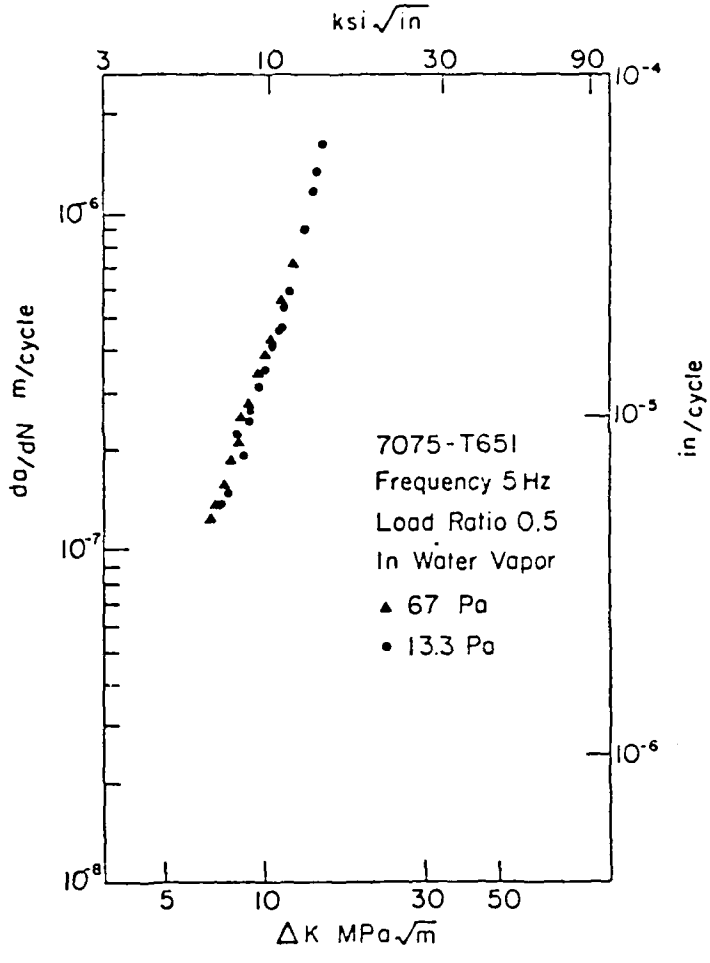

Fig. 7: Effect of water vapor pressure on fatigue crack growth kinetics for I/M 7075-T651 (f = 5 Hz, R = 0.5).

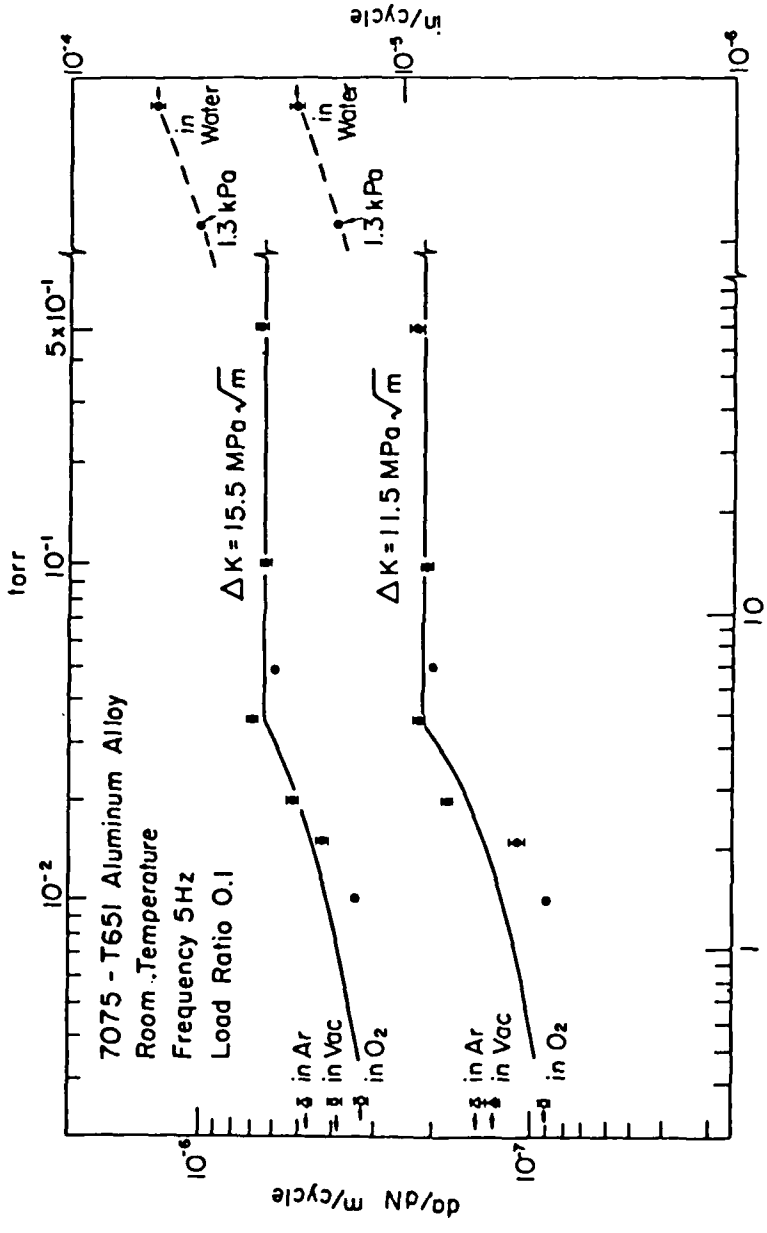

Fig. 8: The influence of water vapor pressure on the fatigue crack growth rate in I/M 7075-T651 aluminum alloy.

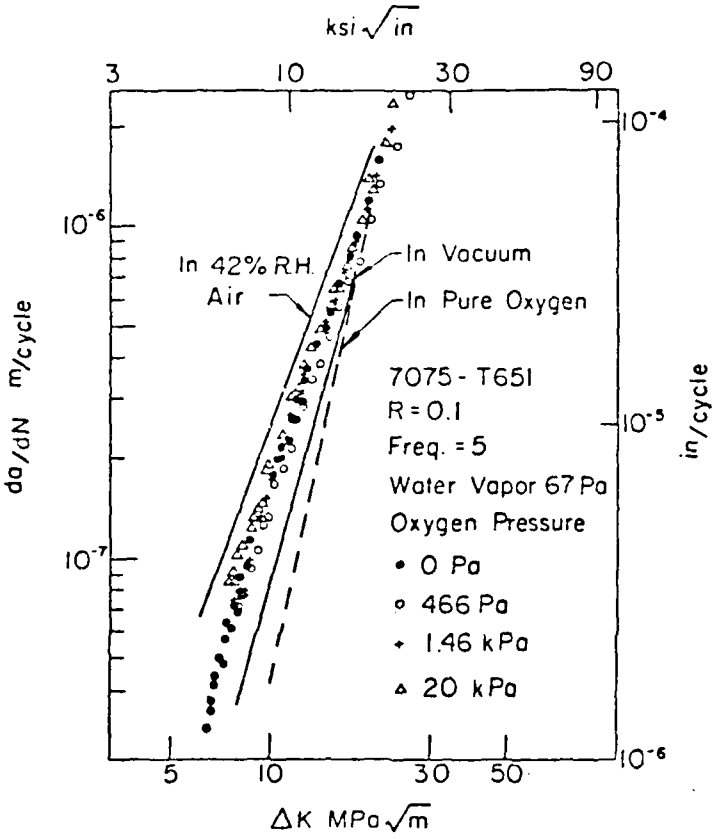

Fig. 9: Effect of oxygen pressure on fatigue crack growth kinetics in a binary gas mixture (P_{H_2O} = 67 Pa) for I/M 7075-T651 aluminum alloy.

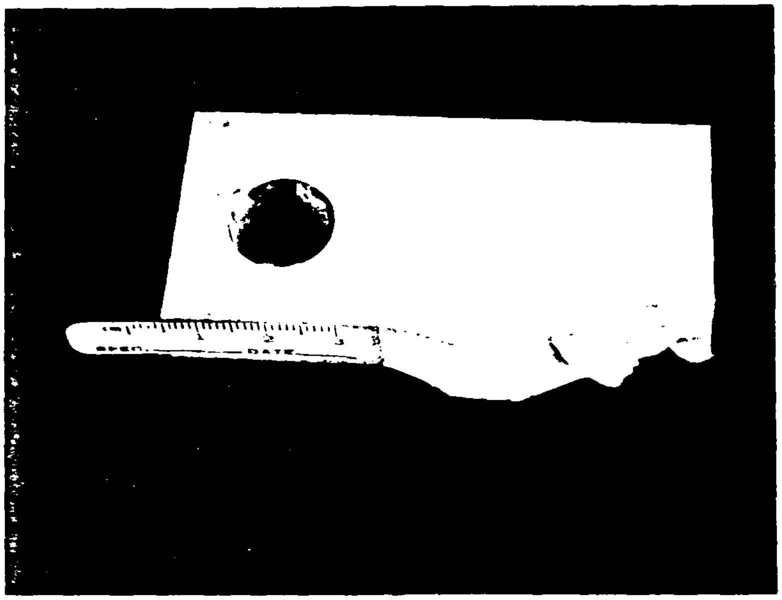

(a)

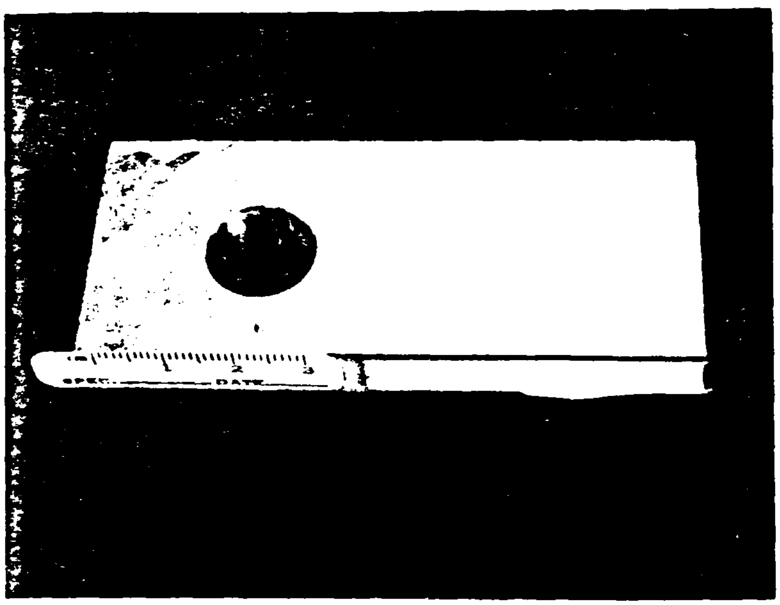

(b)

Fig. 10: Half of [illegible] fracture specimens: (a) [illegible] specimen, [illegible] (b) [illegible] specimen.

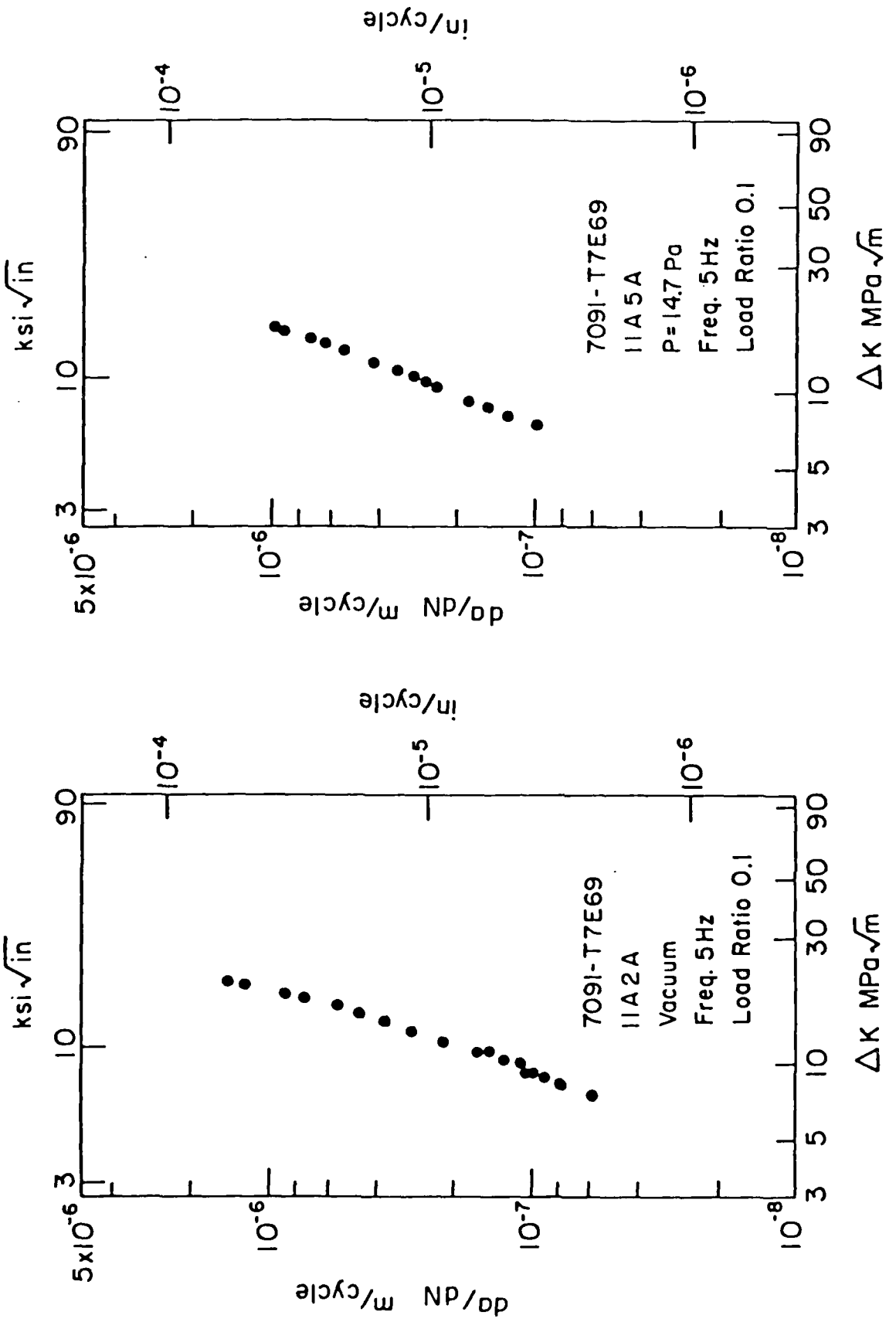

Fig. 11: Kinetics of fatigue crack growth for P/M 7091-T7E69 aluminum alloy (f = 5 Hz, R = 0.1): (a) in vacuum, and (b) in water vapor at 14.7 Pa.

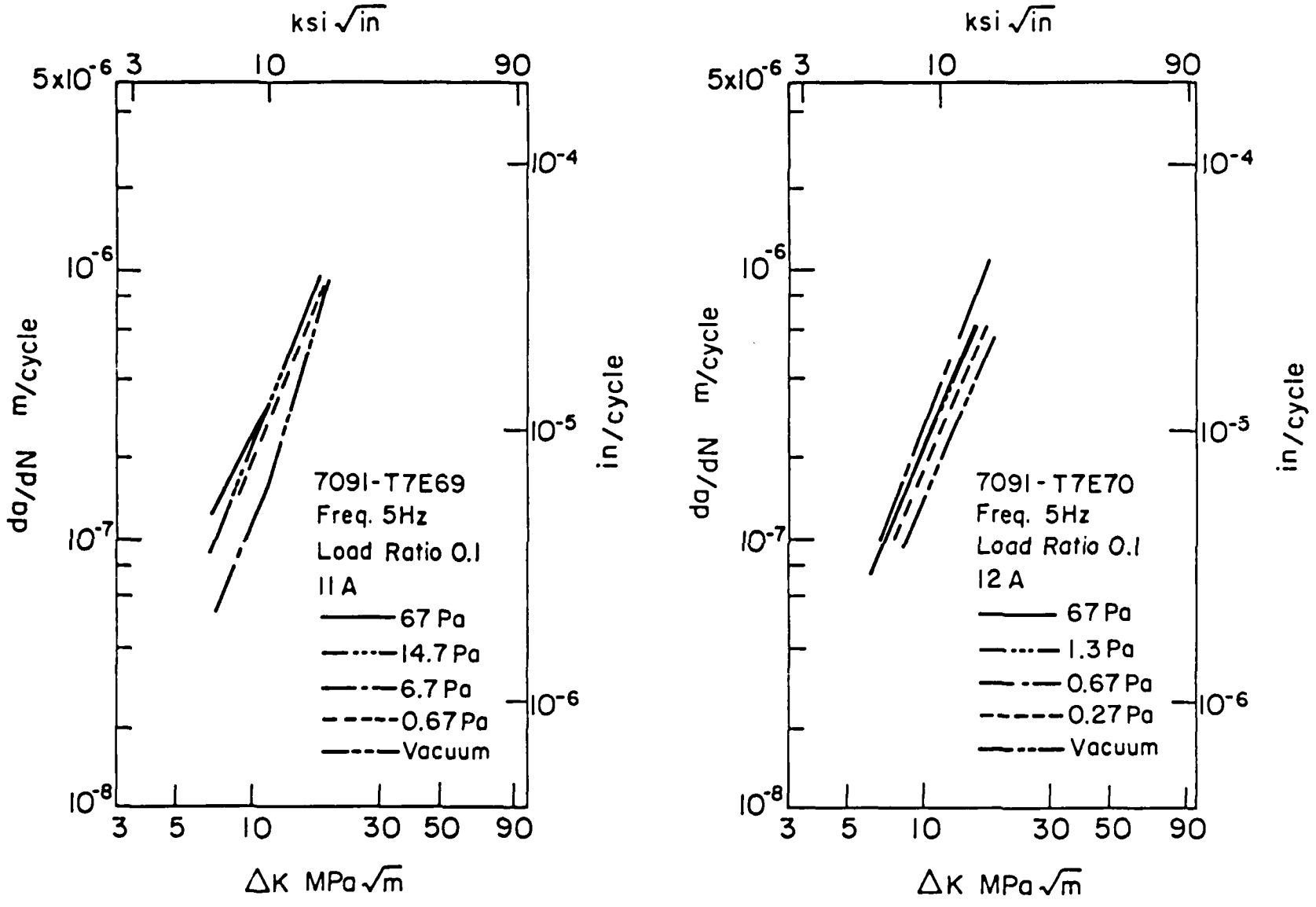

Fig. 12: Comparisons of kinetics of fatigue crack growth in 7091-T7E69 and in 7091-T7E70 aluminum alloys tested in vacuum and water vapor environments: (a) 7091-T7E69, and (b) 7091-T7E70.

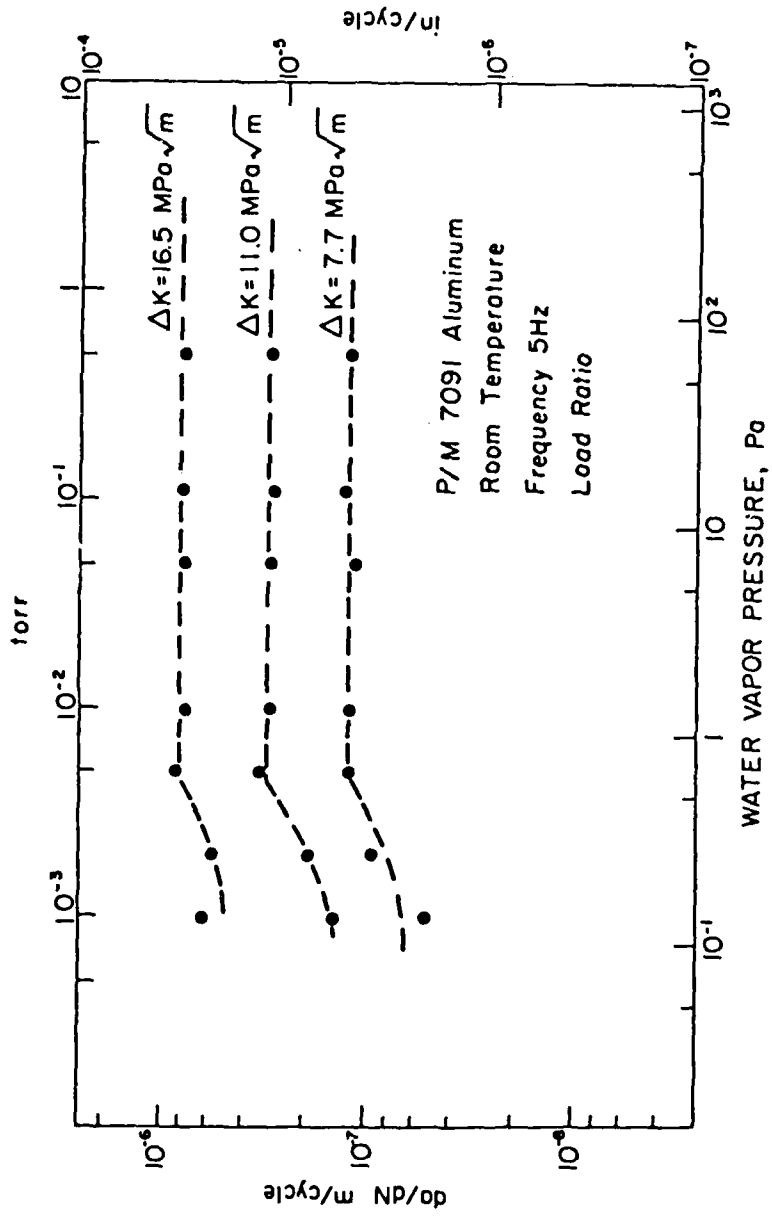

Fig. 13: Influence of water vapor pressure on the fatigue crack growth rate in P/M 7091 aluminum alloy.

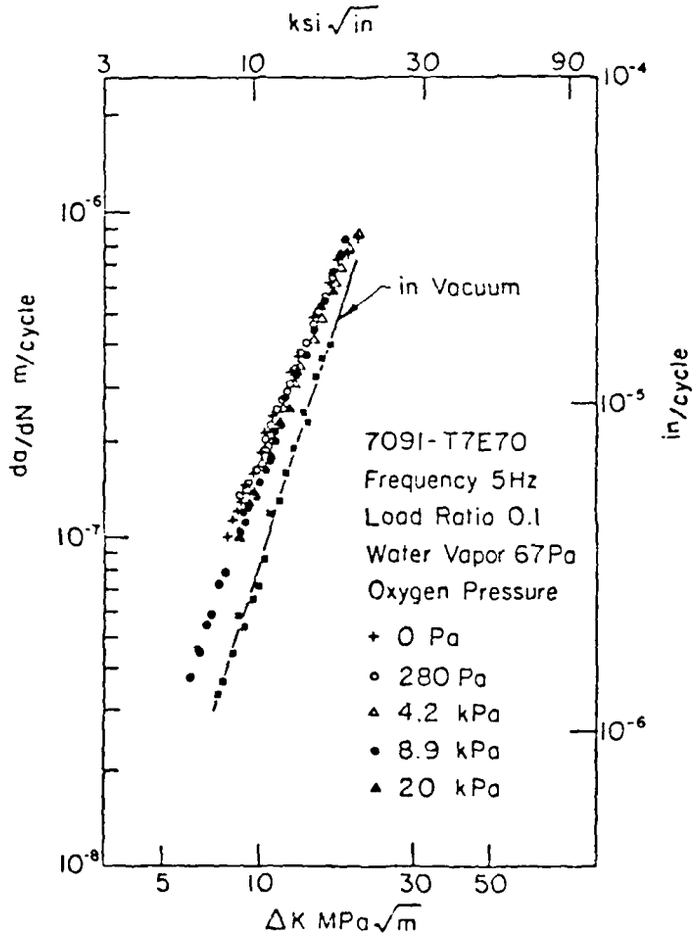

Fig. 14: Effect of oxygen pressure on fatigue crack growth in a binary gas mixture (P_{H_2O} = 67 Pa) for 2.3M 7091-T7E70 aluminum alloy.

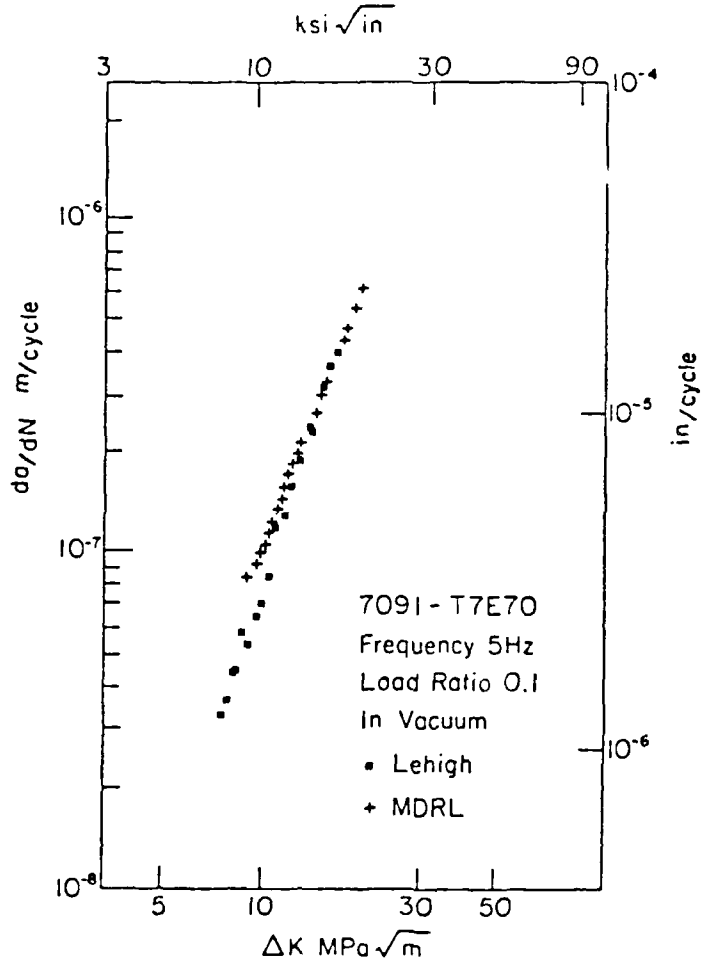

Fig. 15: Comparison of kinetics data of fatigue crack growth experiments in vacuum on P/M 7091-T7E70 aluminum alloy conducted at LU and MDRL.

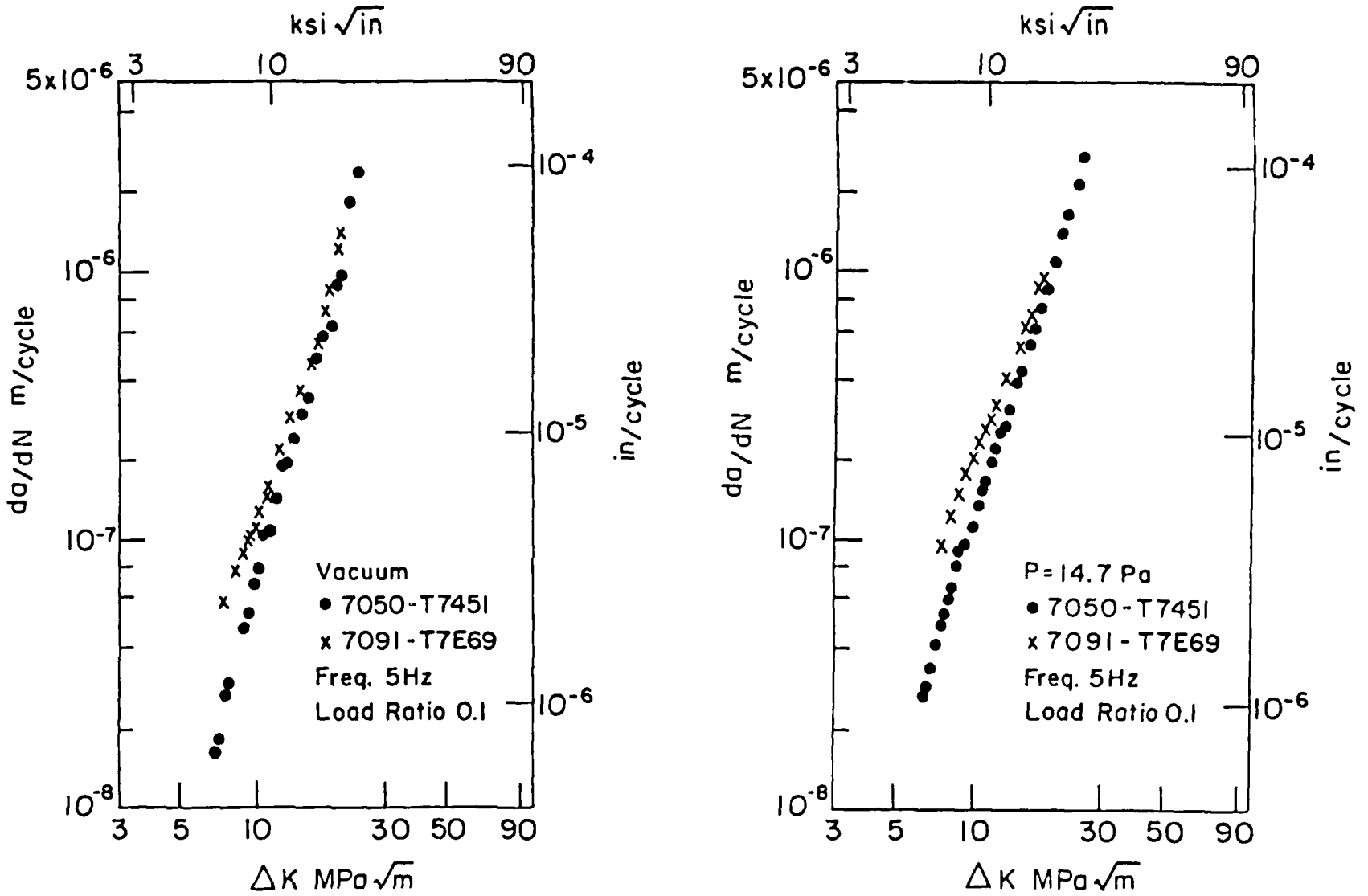

Fig. 16: Comparisons of the kinetics of fatigue crack growth in I/M 7050-T7451 and in P/M 7091-T7E69 in (a) vacuum and (b) 14.7 Pa water vapor.

Fig. 17: SEM microfractographs of I/M 7075-T651 specimen tested in vacuum (ΔK = 11 MPa$\sqrt{m}$, f = 5 Hz, R = 0.1), at low magnification, 200 X.

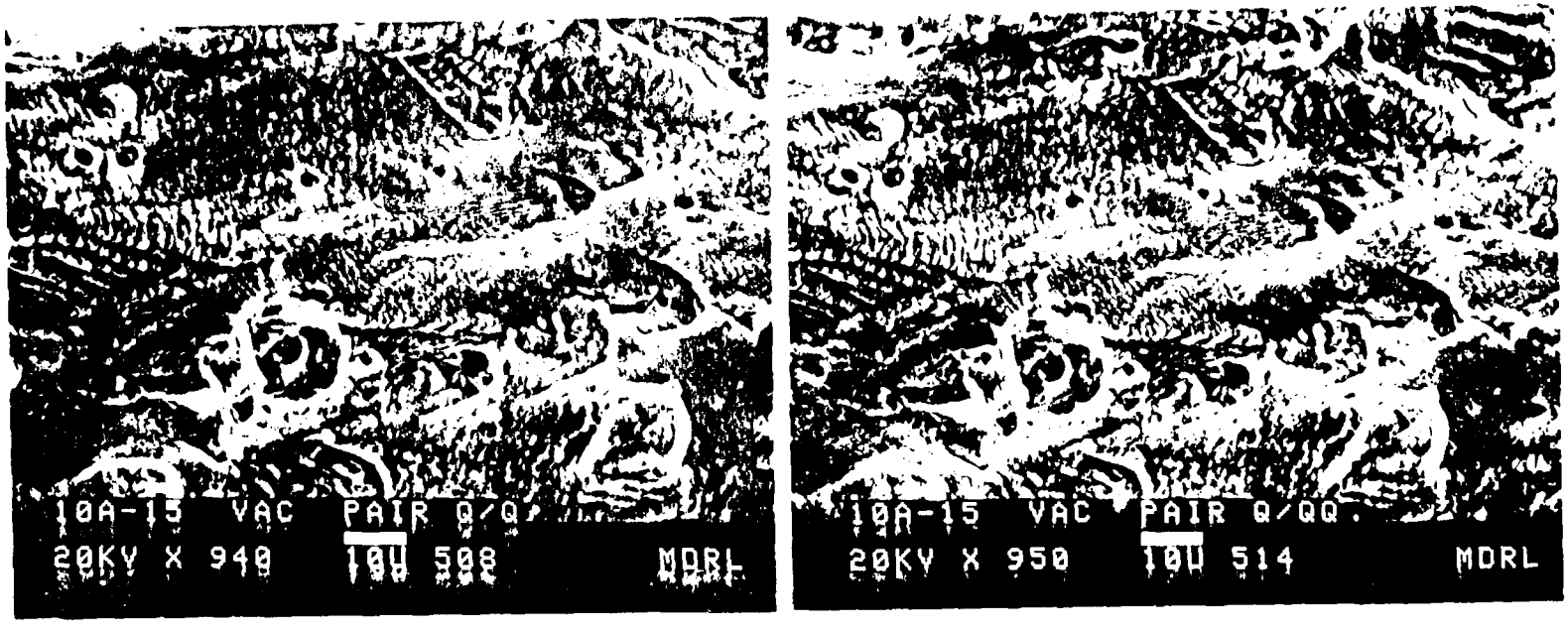

... 12: Stereo pair of the fracture surface morphology for 7075-T651 tested in ... The stereo pair of the mating half is shown in Fig. 20. 950 X

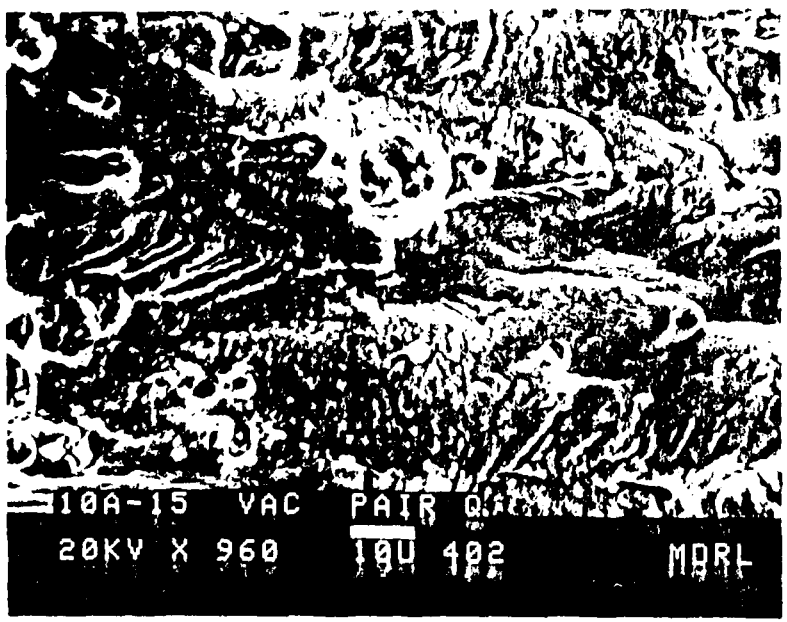

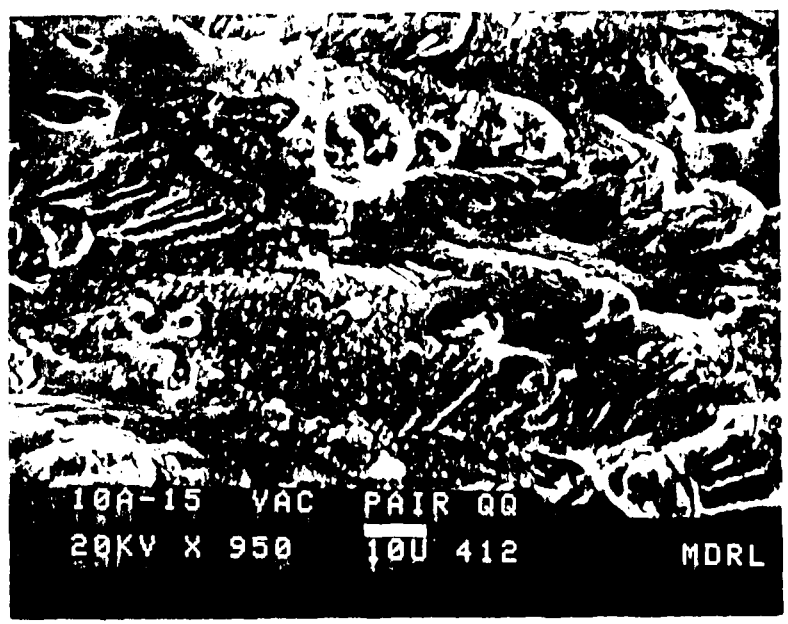

Fig. 20: Stereo pair of the fracture surface morphology for 7075-T651 tested in vacuum. The stereo pair of the mating half is shown in Fig. 19.

(a)

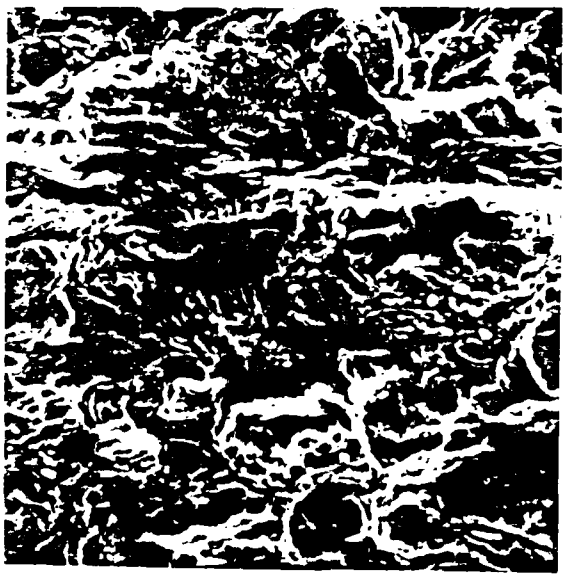

(b)

Fig. 21: SEM microfractographs of I/M 7075-T651 specimen tested in pure oxygen at 266 Pa (ΔK = 11 MPa$\sqrt{m}$, f = 5 Hz and R = 0.1). a) 300 X, b) 600 X

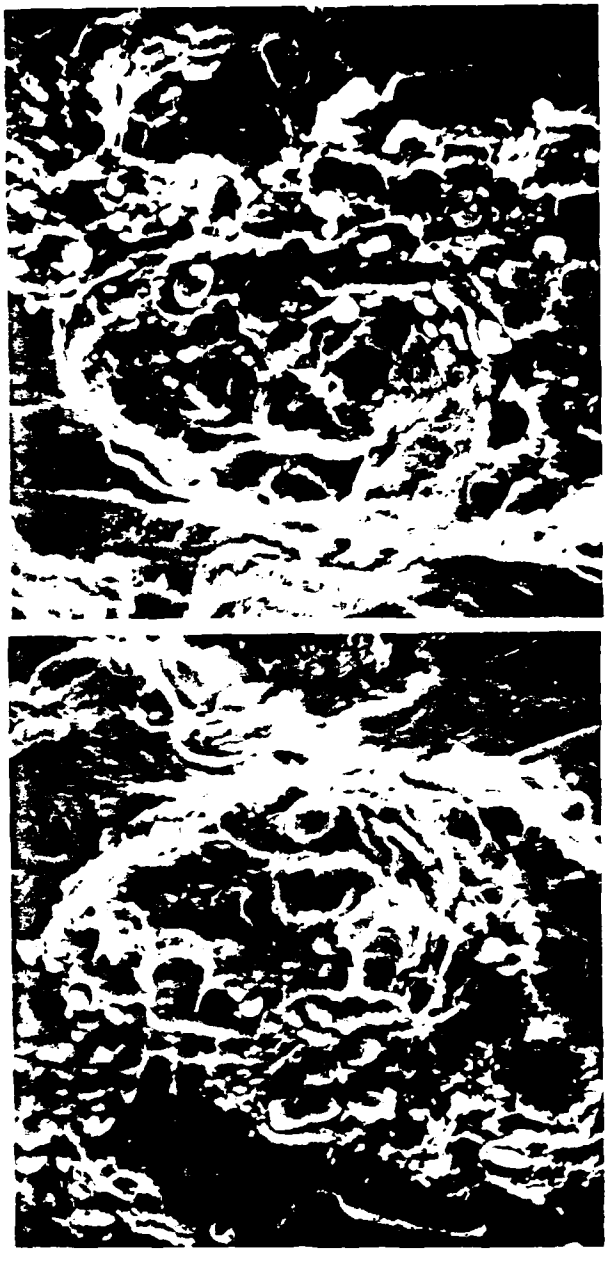

Fig. 22: SEM microfractographs from matins fracture sur-
faces showing particle-hole pairs. EDX spectrum
shows that these particles are iron-rich.

Region A Border Region B

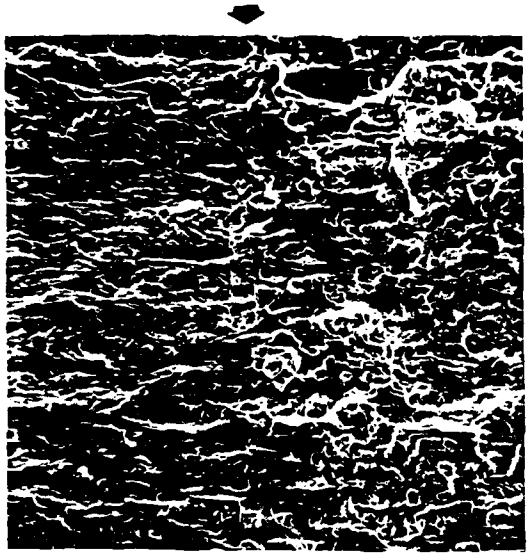

(a)

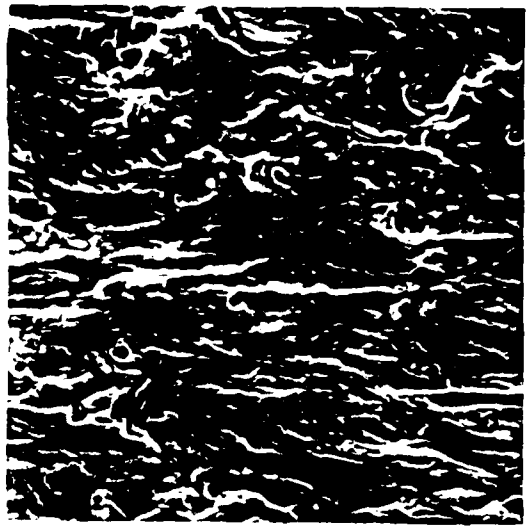

(b)

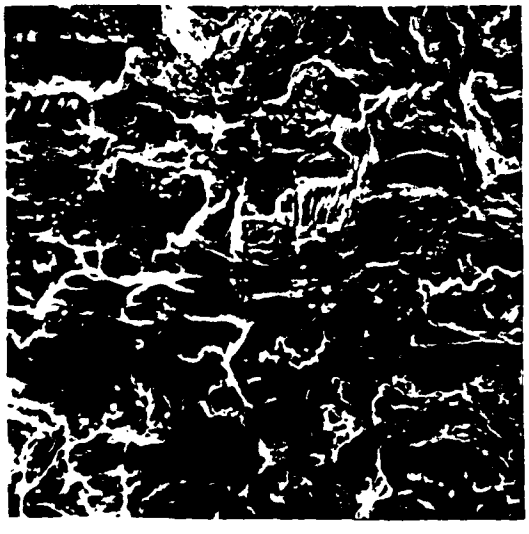

(c)

Fig. 23: SEM microfractographs of I/M 7075-T651 specimen tested in water vapor at 1.3 Pa and 670 Pa (ΔK = 11 MPa$\sqrt{m}$, f = 5 Hz, and R = 0.1) showing differences in fracture surface morphology. a) low magnification, 200 X, Region A tested at 670 Pa and Region B at 1.3 Pa; b) 600 X in Region A, corrosion fatigue component, and c) 600 X in Region B, near "pure" mechanical fatigue component.

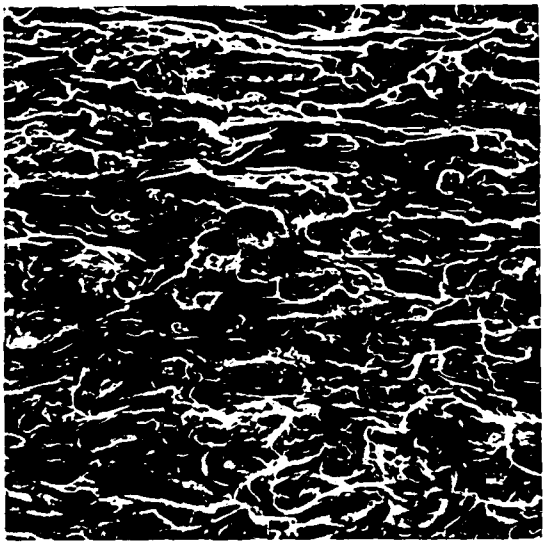

(a)

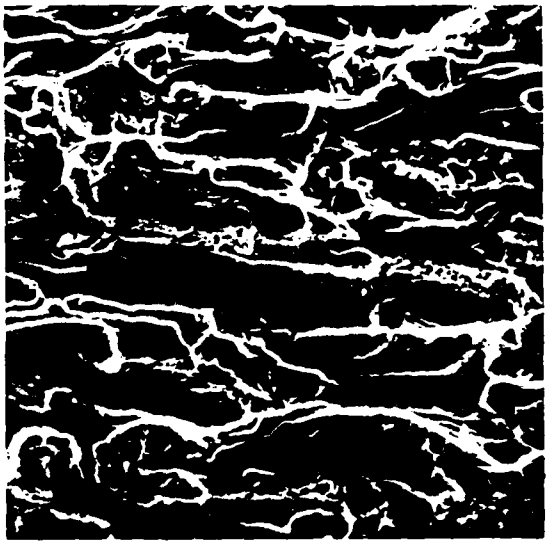

(b)

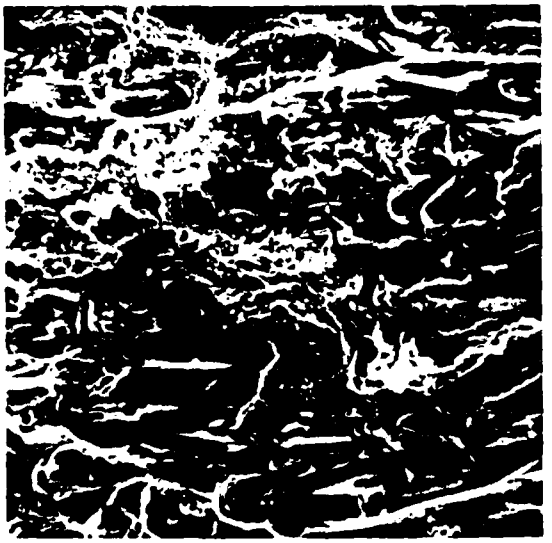

(c)

Fig. 24: SEM microfractographs of I/M 7075-T651 specimen tested in water vapor at 2.6 Pa (ΔK = 11 MPa$\sqrt{m}$, f = 5 Hz, and R = 0.1). a) 300 X, b) 600 X, showing corrosion fatigue component, c) 600 X, showing mechanical fatigue component

(a)

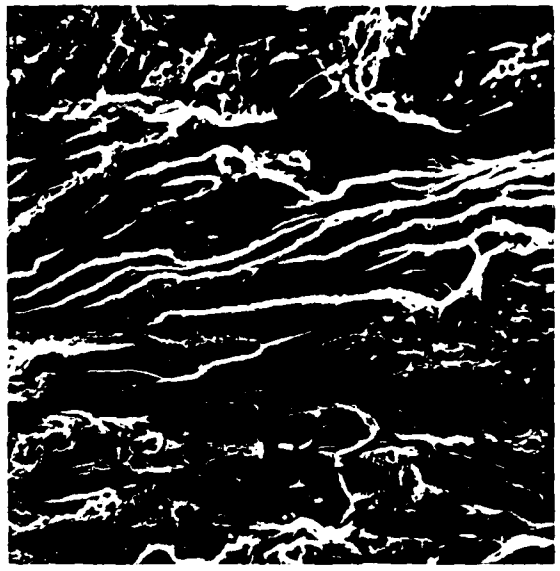

(b)

(c)

Fig. 25: SEM microfractographs of I/M 7075-T651 specimen tested in water vapor at 4.7 Pa (ΔK = 11 MPa$\sqrt{m}$, f = 5 Hz, and R = 0.1). a) 300 X, b) 600 X, showing corrosion fatigue component, and c) 600 X, showing mechanical component.

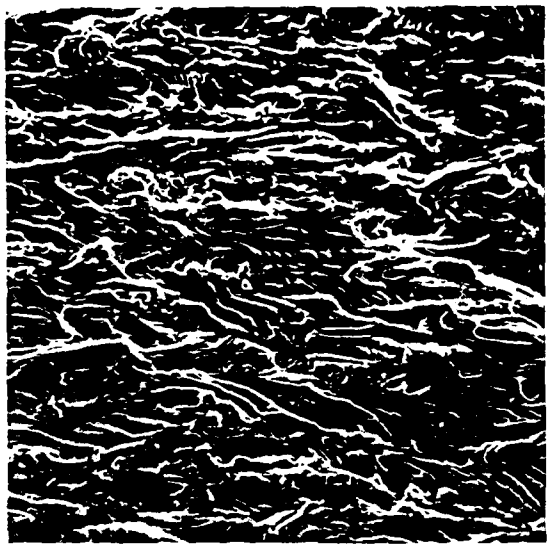

(a)

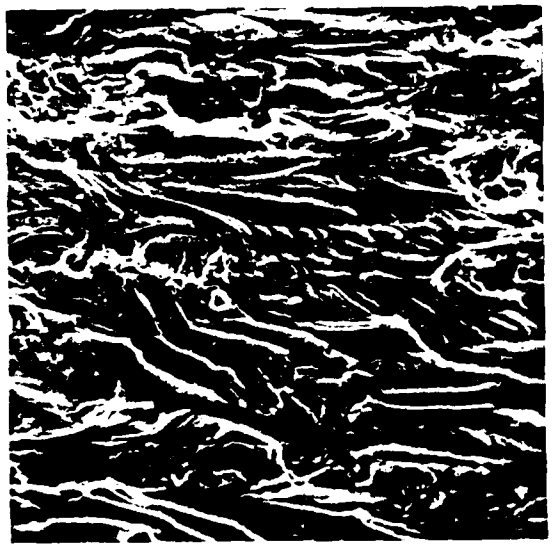

(b)

Fig. 26: SEM microfractographs of I/M 7075-T651 specimen tested in water vapor at 67 Pa. (ΔK = 11 MPa$\sqrt{m}$, f = 5 Hz, and R = 0.1.) a) 300 X, b) 600 X

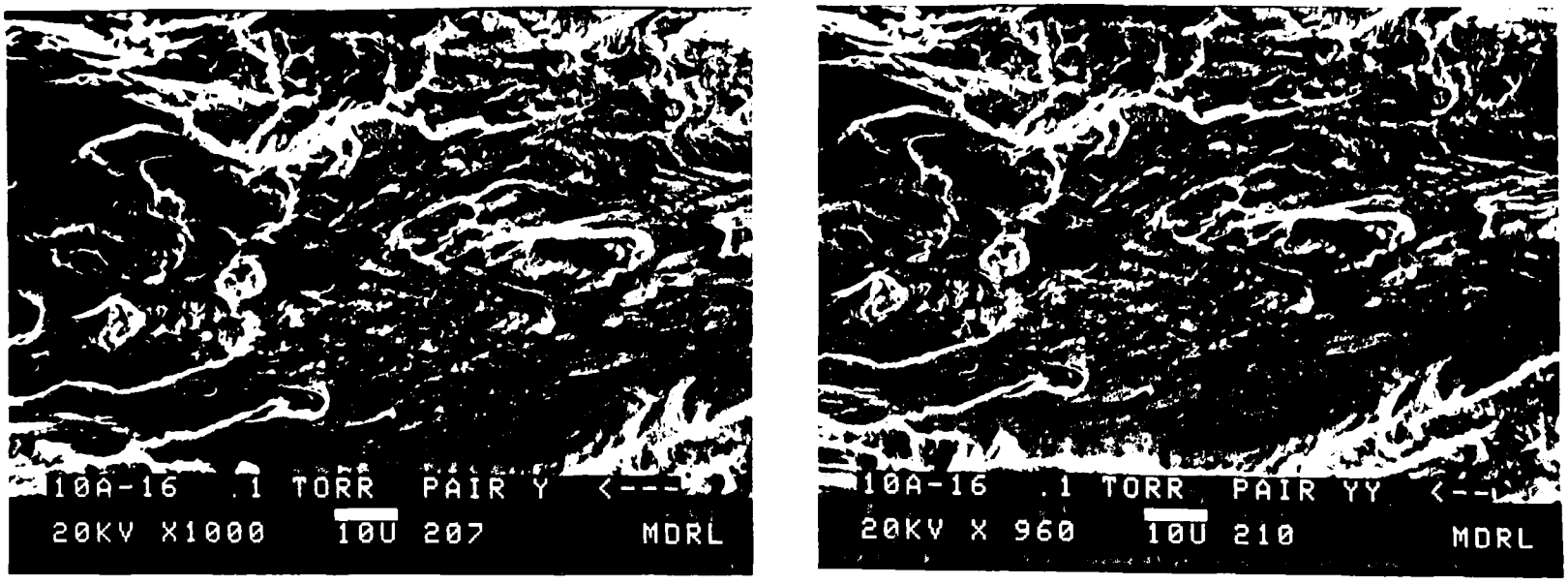

Fig. 27: Stereo pair of the fracture surface morphology for 7075-T651 tested in 13.3 Pa water vapor. The stereo pair of the mating half is shown in Fig. 15.

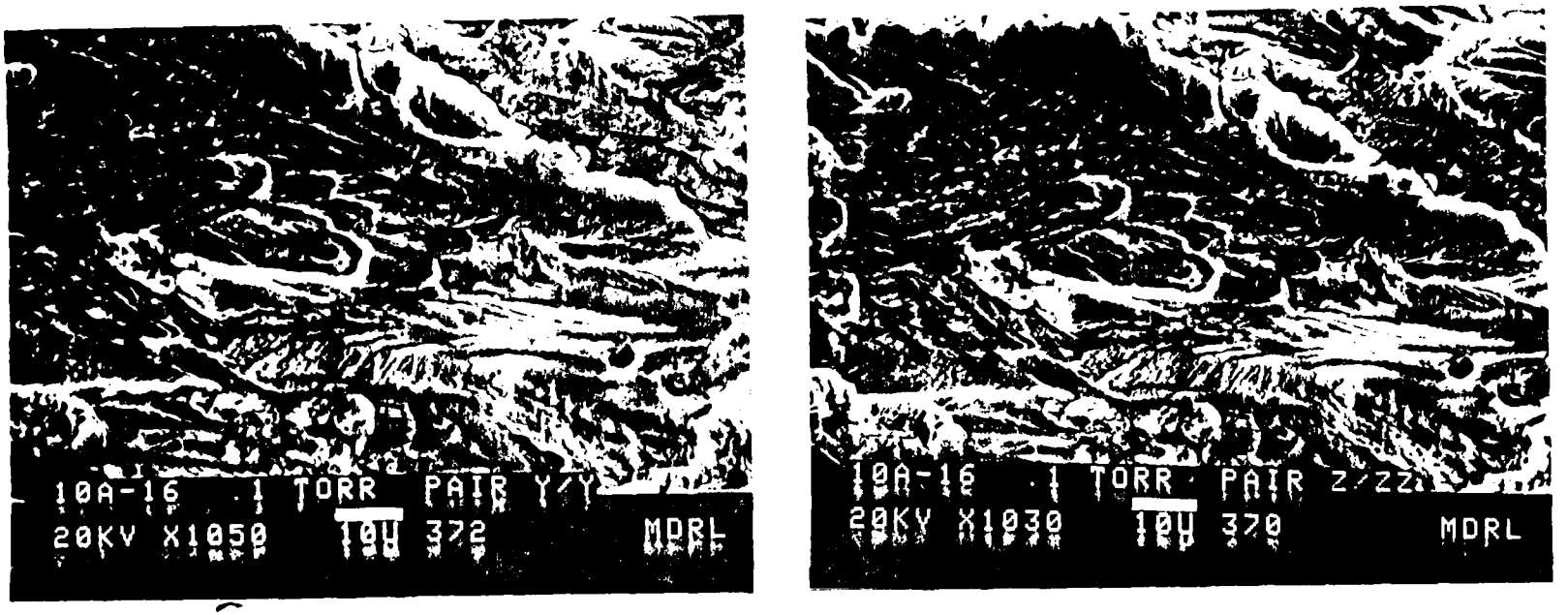

Fig. 28: Stereo pair of the fracture surface morphology for 7075-T651 tested in 13.3 Pa water vapor. The stereo pair of the mating half is shown in Fig. 14.

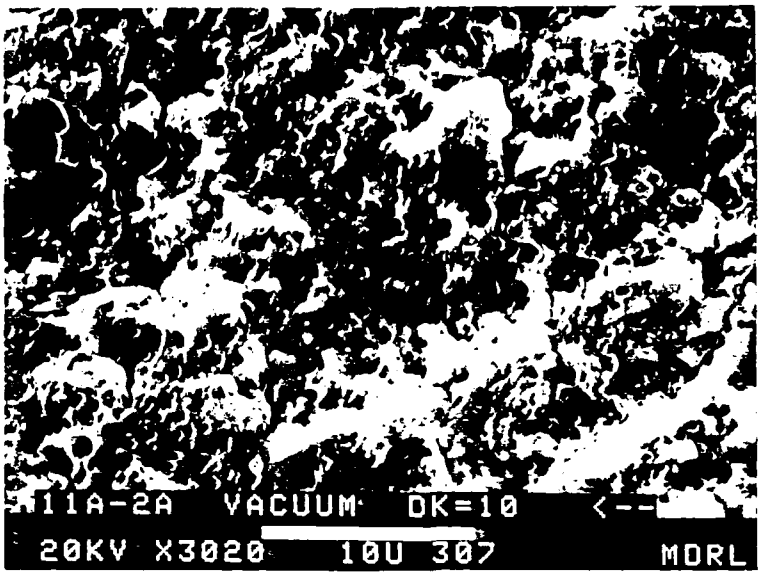

(a)

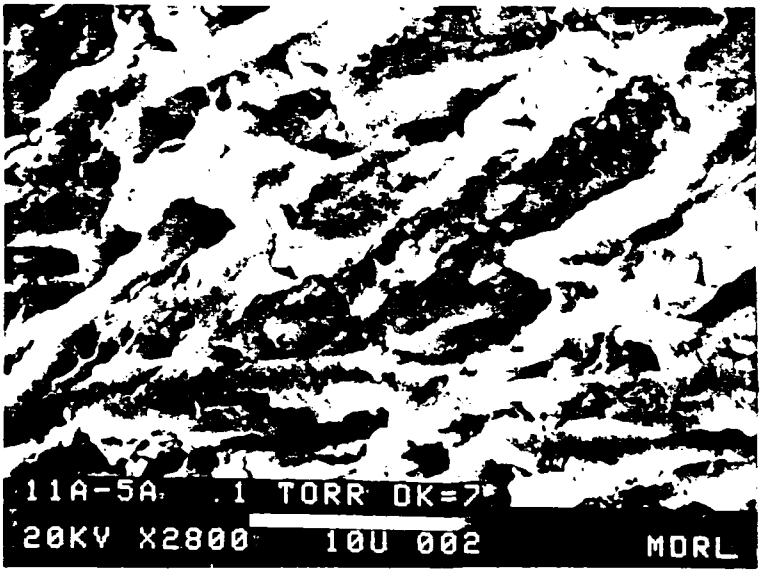

(b)

Fig. 29: SEM microfractographs of P/M 7091-T7E69 tested in (a) vacuum, and (b) 13.3 Pa water vapor (f = 5 Hz, R = 0.1).

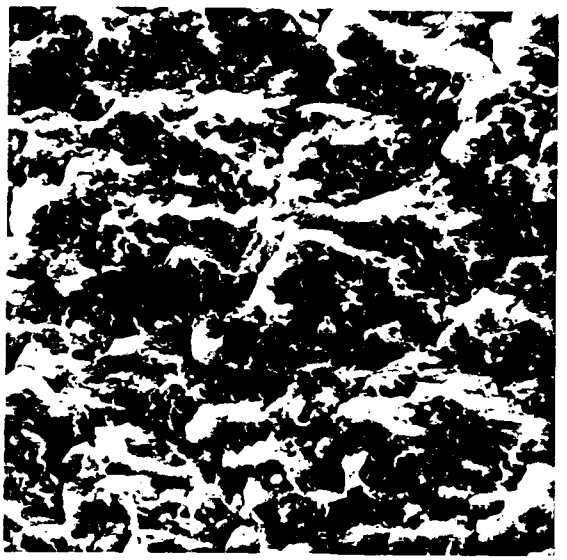

(a)

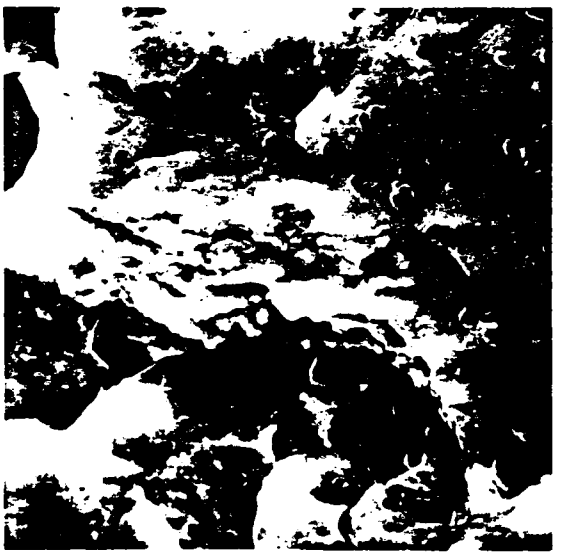

(b)

Fig. 20: SEM microfractographs of P/M 7091-T7E70 tested in pure oxygen (f = 5 Hz, R = 0.1, ΔK = 11 MPa$\sqrt{m}$). a) 1,300 X, b) 5,000 X

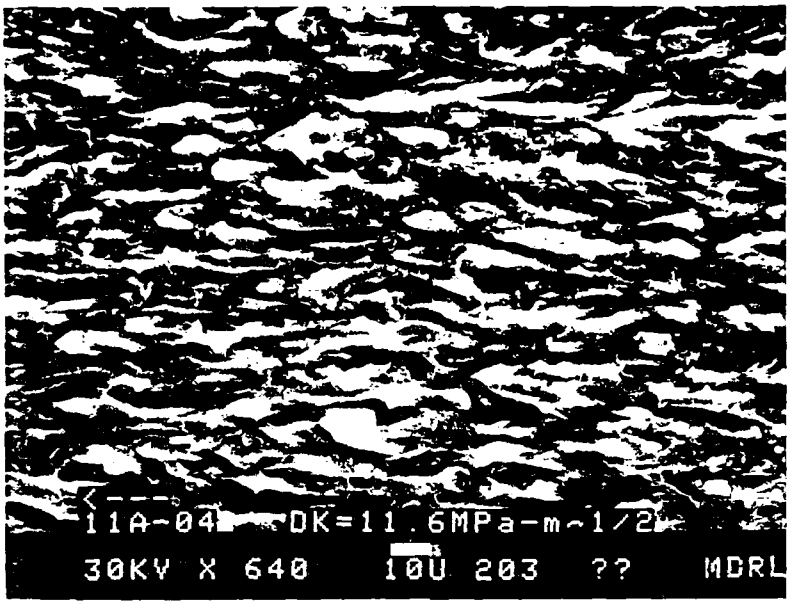

(a)

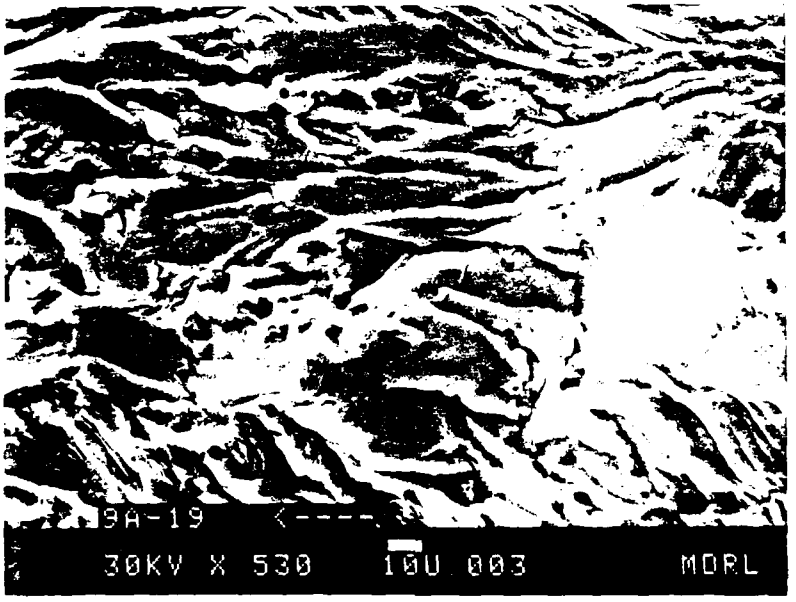

(b)

Fig. 31: Comparison of the fracture surface morphology of (a) P/M 7091-T7E69 and (b) I/M 7050-T7451. Both specimens were fatigue tested in water vapor environment (f = 5 Hz, R = 0.1).

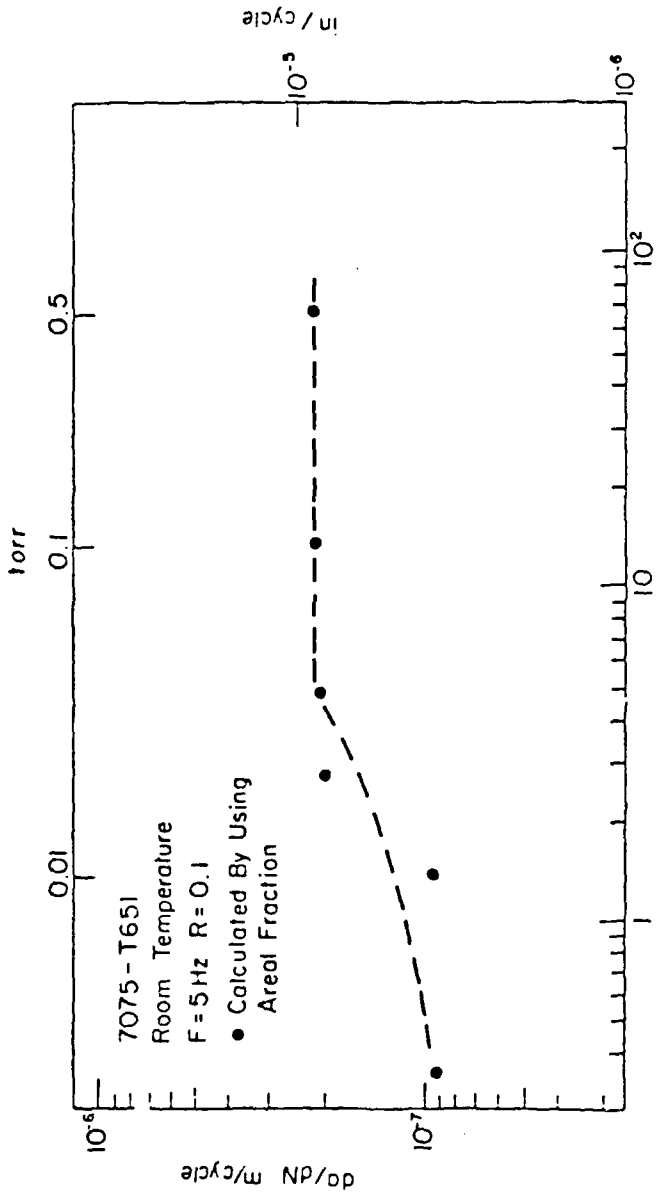

Fig. 32: Comparison between measured rates (dashed lines) of fatigue crack growth and calculated rates (•) from Eqn. (2) using the estimated areal fraction of corrosion fatigue, ϕ.

DISTRIBUTION LIST

January, 1982

Mr. Alan Rosenstein
AFOSR/NE
U. S. Air Force Office of Scientific Research
Bolling Air Force Base
Washington, DC 20332 (6)

AFWAL/MLLS
Attn: Dr. Terry Ronald (1)
Dr. Walt Griffith (1)
Dr. F. H. Froes (1)
Dr. William Baeslack (1)
WPAFB, Ohio 45433

Prof. I. M. Bernstein (1)
Dept. of Metallurgy/Material Science
Carnegie-Mellon University
Pittsburgh, PA 15213

Mr. Walter Cebulak (1)
Alcoa Technical Center
Alloy Technology Division
Alcoa Center, PA 15069

Dr. David L. Davidson (1)
Mechanical Sciences Dept.
Southwest Research Inst.
San Antonio, TX 78284

Prof. Morris E. Fine (1)
Dept. of Materials Science
Northwestern University
Evanston, IL 60201

Lt. Col. Loren Jacobson (1)
DARPA
Material Sciences Div.
1400 Wilson Blvd.
Arlington, VA 22209

Prof. Michael J. Koczak (1)
Dept. of Materials Engineering
Drexel University
Philadelphia, PA 19104

Dr. James Lankford, Jr. (1)
Mechanical Sciences Dept.
Southwest Research Inst.
San Antonio, TX 78284

Prof. Alan Lawley (1)
Dept. of Materials Engineering
Drexel University
Philadelphia, PA 19104

Prof. Art McEvily (1)
Dept. of Metallurgy
University of Connecticut
Storrs, CT 06268

Mr. Henry Paris (1)
Alcoa Technical Center
Alloy Technology Division
Alcoa Center, Pa 15069

Dr. Neil Paton (1)
Rockwell Science Center
Thousand Oaks, CA 91360

Prof. Thomas Sanders (1)
Purdue University
School of Materials Engineering
Chemical Metallurgy Engineering Building
West Lafayette, IN 47907

Dr. J. S. Santner (1)
Materials Research Lab., Inc.
One Science Road
Glenwood, IL 60425

Dr. Shankar M. L. Sastry (1)
McDonnell Douglas Res. Lab.
St. Louis, MO 63166

Mr. James Staley (1)
Alcoa Technical Center
Alloy Technology Division
Alcoa Center, PA 15069

Prof. E. A. Starke, Jr. (1)
Dept. of Chemical Engineering
Georgia Institute of Technology
Atlanta, GA 30332

Prof. A. W. Thompson (1)
Dept. of Metallurgy/Material Sci.
Carnegie-Mellon University
Pittsburgh, PA 15213

Prof. Julia R. Weertman (1)
Dept. of Materials Science
Northwestern University
Evanston, IL 60201

Prof. R. P. Wei (1)
Dept. of Mechanical Engineering & Mechanics
Lehigh University
Bethlehem, PA 18015

END

DATE
FILMED

7-83

DTIC